



**Stochastic Sizing and Operation of Grid-Level Energy Storage Systems
under Intermittent Renewable Generation and Increasing Load
Forecasting Uncertainties**

**Prepared for the U.S. DOE Office of Electricity
Advanced Grid Modeling (AGM) Program
Program Manager: Dr. Alireza Ghassemian**

by

Meng Yue^a, Tianqiao Zhao^a, Niranjana Raghunathan^b, Peter Luh^b, Bing Yan^c, and
Mikhail Bragin^b

^aInterdisciplinary Science Department, Brookhaven National Laboratory

^bDepartment of Electrical and Computer Engineering, University of Connecticut

^cDepartment of Electrical and Microelectronic Engineering, Rochester Institute of
Technology

July 31, 2021

Table of Contents

Acronyms	v
Nomenclature	vi
Executive Summary	viii
1. Introduction	1
2. Overview of Methodology Development	4
2.1 Uncertainty Modeling	4
2.1.1 A Markovian Approach for ESS Operation Studies	5
2.1.2 Random Field Approach for ESS Planning Studies	5
2.2 Constraint Tightening	6
2.3 SAVLR with Soft Constraints	7
3. ESS Planning Study	8
3.1 Problem Formulation	8
3.1.1. Objective Function	8
3.1.2. System Constraints	8
3.1.3. Frequency Dynamics Security Under Contingencies	9
3.1.3.1 Rate of Change of Frequency (RoCoF)	9
3.1.3.2 Frequency Nadir Constraints	10
3.1.3.3 Quasi-steady-state Frequency Constraints	11
3.1.4. Model Linearization	12
3.2 Scenario Development	14
3.3 Solutions	15
3.3.1. Incorporating Rolling Horizon to SAVLR	16
4 ESS Operation Study	18
4.1 Problem Formulation	18
4.1.1 ESS operation with Frequency Dynamics Constraints in a Deterministic Setting	18
4.1.1.1 Objective Function	18
4.1.1.2 System Constraints	18
4.1.2 ESS Operation with Frequency Dynamics Constraints in a Stochastic Setting	19
4.1.2.1 Objective Function	19
4.1.2.2 System Constraints	19
4.2 Scenario Development: Markov Model for Wind Generation	19

4.3	Solution	20
4.3.1	Solution to Deterministic ESS Operation with FDUC	20
4.3.2	Solution to Stochastic ESS operation with FDUC	20
5	Tool Implementation	23
5.1	Overall Architecture of SAVLR and SAVLRseq	23
5.2	Software Requirements	25
5.3	Quick Start Guide	25
5.4	Improving Performance of MATALB Code.....	26
6.	Case Study	27
6.1	Example Systems	27
6.2	ESS Operation Case Study	27
6.2.1.	ESS Operation in a Deterministic Wind Generation Setting	27
6.2.2.	ESS Operation for the Markovian wind generation model.....	28
6.3	ESS Planning Case Study.....	29
6.3.1.	Test Systems and Data	29
6.3.2.	Tuning Parameters	30
6.3.3.	Results.....	30
6.3.3.1.	IEEE 118-bus System: 24-hour Planning Problem	30
6.3.3.2.	IEEE 118-bus System: One-year Planning Problem	31
6.3.3.3.	Scalability Study in the 2,383-bus Polish System: 24-hrs Planning Problem.....	33
6.3.3.4.	Scalability study in the 2,383-bus Polish system: One-year planning problem	34
7.	Conclusions and Future Work	35
	References:	37

Table of Figures

Figure 1: An Example of Concurrent Reduction in Generation of Two Highly Correlated Wind Farms	4
Figure 2: The NDM for bivariate random field.	6
Figure 3: Flowchart of SAVLR	7
Figure 4. Illustration power mismatch and frequency dynamics.	10
Figure 5. Illustration of linearization of $y \geq x^2$.	13
Figure 6: Histogram for wind speed at three wind sites.	14
Figure 7: The time series data of the simulation.	15
Figure 8: Histograms of simulated data and assumed distribution.	15
Figure 9: The flowchart of SAVLR+rolling horizon (SAVLRseq).	16
Figure 10: Example Markov chain for wind generation states for 2 hours, where $t = 0$ represents the initial distribution. This model has 9 global states (can also be considered as generation levels).	20
Figure 11: Active states and transitions after the first iteration of the OO filtering algorithm	21
Figure 12: Active states and transitions after 3 iterations of the OO filtering algorithm	21
Figure 13: SAVLR flowchart with OO approximation for subproblems	22
Figure 14: Structure of the open-source ESS Sizing Tool.	24
Figure 15: Contents of the SAVLR code for MFDUC	25
Figure 16: Define algorithm settings in SAVLR_RUN.m	26
Figure 17: a) parallel for loop is used for constructing subproblem models in the preprocessing stage. b) The RoCoF constraints are built using vectorization and stored in a sparse matrix.	26
Figure 18: Diagram for the 118-bus system.	27
Figure 19: Aggregated state-of-charge of ESSs for the deterministic FDUC	28
Figure 20: Wind generation obtained by Random Filed.	30
Figure 21: Results for 24hrs planning with ESS support.	31
Figure 22: Results for 24hrs planning without ESS for frequency support.	31
Figure 23: Figure 4. Results for one-year planning with ESS for frequency support	33
Figure 24: Results for 24-hrs planning with ESS for frequency support.	34

Table of Tables

Table 1: Wind Farm Correlation vs. Percentage of Concurrent Changes in Generation of Two Wind Farms	4
Table 2: Mean and standard deviation of historical wind speed data.	14
Table 3: The estimated cross-correlation coefficients of the original data.	14
Table 4: The difference between the estimated cross-correlation coefficients of the simulated data and original data (Corr_original – Corr_simul).	15
Table 5: The Functionality of Modules	24
Table 6: Results from SAVLR+OO for the Markovian FDUC	28
Table 7: Comparison of different parameters for the 3-hrs planning problem ($\gamma = 0.1$).	30
Table 8: Comparison of different solutions for the one-month planning problem.	32
Table 9: Comparative results of SAVRLseq with different time slots.	32
Table 10: Comparison of different solutions for the one-year planning problem in 118-bus system. ...	32
Table 11: Comparison of different solutions for the one-year planning problem in Polish system.	34

Acronyms

ARMA	Auto Regressive Moving Average
BESS	Battery Energy Storage System
ESS	Energy Storage System
FN	Frequency nadir
ICDF	Inverse Cumulative Distribution Function
MILP	Mixed Integer Linear Programming
MPPT	Maximum Power Point Tracking
NDM	Nataf's joint Distribution Model
QSS	Quasi-steady state
RV	Random Variable
RFT	Random Field Theory
RF	Random Field
RoCoF	Rate-of-change-of-frequency
SAVLR	Surrogate Absolute Value Lagrangian Relaxation
SLR	Surrogate Lagrangian Relaxation
SOC	State of Charge
UC	Unit Commitment

Nomenclature

Superscripts, subscripts, and sets

Ω_B, i	Set and index of buses $\{1, \dots, n_b\}$
Ω_E	Set of energy storage system (ESS) index $\{1, \dots, n_E\}$ (let $n_E = n_b$)
Ω_G	Set of conventional generators index $\{1, \dots, n_G\}$
Ω_L	Set of right-of-ways $\{1, \dots, n_l\}$
Ω_A	Set of areas $\{1, \dots, n_a\}$
Ω_{Gb}	Set of generators at bus b $\{1, \dots, n_i\}$
Ω_{Eb}	Set of ESSs at bus b $\{1, \dots, n_E\}$
Ω_H	Set of branches for the operation problem $\{1, \dots, n_h\}$
Ω_D	Set of power generation blocks $\{1, \dots, n_d\}$
Ω_M	Set of global states in the Markov model $\{1, \dots, n_m\}$
Ω_Q	Set of reserve types, i.e., Regulation, 10-min synchronous, 10-min non-synchronous, 30-min synchronous, and 30-min non-synchronous $\{1, \dots, n_q\}$
Ω_O	Set of global states in the ordinal optimization approximation for subproblems $\{1, \dots, n_o\}$
Ω_R	Set of reserve classes, i.e., Regulation, 10-min synchronous, 10-min total, and 30-min total $\{1, \dots, n_r\}$
Ω_{Wb}	Set of windfarms at bus b $\{1, \dots, n_w\}$
Ω_T, t	Set $\{1, \dots, n_t\}$ and index of time
Ω_W	Set of renewable (wind farm) index $\{1, \dots, n_w\}$
$\Omega_\omega,$	Set and index of scenarios
ω	
Ω_κ, κ	Set and index of contingencies
Ω_j	Set $\{0, 1, \dots, n_j\}$

Parameters

$c_i^g, c_i^{SU}, c_i^{NL}$	Cost coefficients of conventional generators: generation, startup, and no-load cost, respectively
c_i^{ls}/c_i^{rs}	Cost coefficients of load/renewable shedding
c_i^E	Cost coefficient of ESS energy cost
Pd_i^ω	Load demand
f_{db}	Governors' dead band
f_0	System normal frequency (60 Hz)
f_{MIN}	Pre-specified frequency lower limit
$\underline{f}_{ij}/\bar{f}_{ij}$	Lower/upper limit of branch capacity
$\underline{Pg}_i/\bar{Pg}_i$	Lower/upper output limit of generator i
p_ω	Probability of scenario ω
$Pr_{it}^{o\omega}$	Available capacity of renewable output
t_d	Dead band time of governor
t_{NAD}	Time of system reaching frequency nadir
v_i	Maximum governor ramp rate of generator i (MW/second)
v_{NAD}	Total governor ramp rate of a system
$wd_{it}^\omega, wu_{it}^\omega$	Decreased and increased wind power output, respectively,

DR_i	Droop constant of a generator for primary frequency regulation (set to 0.05)
$H_t^{\omega\kappa}$	System inertia (MWs/Hz) after contingency κ
H_i	Generator inertia (s)
R_t^ω	Required system spinning reserve
RU_i/RD_i	Maximum ramp up/down rate
$RoCoF^{\max}$	Maximum allowable rate of change of frequency
X_{ij}	Reactance of line i-j
Δf_{qss}	The difference between f^0 and quasi-steady-state frequency
Δf_{qss}^{\max}	Maximum allowable value of $\Delta f_{qss}^{\omega\kappa}$ (set to 0.2 Hz)
Δt	Duration time: one hour
$\Delta t_{IR}, \Delta t_{PFR}$	Inertia response time and primary frequency regulation time, respectively
$\eta_i^{ch/dch}$	Charging/discharging efficiencies

Variable

$Pb_{it}^{c,\omega}/Pb_{it}^{d,\omega}$	Charging/discharging power
$Pb_{d,t}^{\omega\kappa}/Pb_{c,t}^{\omega\kappa}$	Increased/decreased power output from ESS immediately after the moment of contingency κ
$Pd_i^{s\omega}, Pr_i^{s\omega}$	Load and renewable shedding, respectively
f_{ij}^ω	Power flow from node i to node j
$Pg_{it}^\omega, Pg_{it}^{R\omega\kappa}$	Output and spinning reserve of conventional generator i , respectively (≥ 0)
u_{it}^ω	On-off status of a conventional generator (binary)
BE_i	Energy capacity of ESS
$Pb_i^{ch/dch}$	Maximum charging/discharging power of ESS
SOC_{it}^ω	State of charge in terms of energy
$SU_{it}^\omega/SD_{it}^\omega$	Startup/shutdown status (binary)
α_{it}/β_{it}	Charging/discharging status indicator (binary)
θ_i^ω	Phase angle of node i
$\Delta f_{qss}^{\omega\kappa}$	Difference between f_0 and quasi-steady-state frequency
$\Delta g_{t,u}^{\omega\kappa}$	Downward system power imbalance (insufficient generation) caused by outages
$\Delta g_{t,o}^{\omega\kappa}$	Upward system power imbalance (excess generation) caused by outages
$\Delta g^{\omega\kappa}$	System power mismatch immediately after the moment of contingency- κ
τ_i^+/τ_i^-	Minimum up/down time

Executive Summary

Background

The objective of this project is to develop a scalable methodology and a practical tool that can be used by utilities to perform unit commitment (UC) based energy storage system (ESS) planning and operation to guarantee a reliable and secure operation of large-scale power systems by satisfying various constraints, including those related to frequency dynamics, under high uncertainties associated with the continually increasing renewables.

Grid inertia provided by conventional synchronous generators plays a vital role in suppressing disturbances that originate both within and outside of the grid. The rapidly increasing penetration of intermittent renewables such as solar and wind displaces the conventional power generation plants, causing a rising concern with the performance of grid responses including frequency issues such as inertial and primary frequency response, especially under light load conditions. Large power mismatches caused by high fluctuations of renewables may further exacerbate grid frequency stability. Loss of inertia is thus a grave concern to grid operators.

A possible means to achieve a healthy frequency response is to use energy storage systems (ESSs). ESSs possess response speeds that are superior to conventional generators and can significantly improve grid responses. In addition, ESSs are beneficial to operations by providing much needed energy, ramping as well as reserve services, especially under high penetration of intermittent renewables.

While the effectiveness of the ESS response is well-known, both the capital and operational costs of ESSs of various technologies is very high and the lifespan of ESSs, especially battery energy storage systems (BESSs) is limited by the total number of charging and discharging cycles. Therefore, the major challenges that need to be addressed before ESS deployment are (1) what are the required capacities of ESSs, i.e., the sizing of ESSs, to achieve desired grid operational performance under different types of credible disturbances; and (2) how to efficiently operate the ESSs to ensure efficiency, security, and reliability of the power grids. The major purpose of this project is to develop revolutionary methodologies to answer these questions for planning and operation of utility-scale systems.

To answer the questions above, this study consists of two closely connected topics, i.e., sizing of ESSs considering constraints such as frequency responses under high penetration of renewables; and stochastic operation optimization of ESSs accounting for the state-of-charge (SOC) and intermittence of renewable generation and the increasing load uncertainties due to, e.g., behind-the-meter renewables (e.g., rooftop PVs). The frequency response-based ESS sizing ensures the frequency stability, while stochastic optimization-based operation ensures efficiently and reliably running of ESSs together with other units on the grid. The study was enabled by the development and implementation of an innovative scalable stochastic optimization method to solve mixed integer linear programming (MILP) problems including utility-scale UC problems.

Probabilistic Sizing of ESSs

There are many challenges that impact the grid security and reliability. It is neither impossible nor necessary (affordable) to plan for the worse case scenarios. Rather, we should consider the consequence of the undesired events as well as the probabilities of the occurrences of such events. Therefore, it is preferred to adopt a probabilistic approach to sizing ESSs in a system, and uncertainty modeling becomes an important part of the study.

The uncertainties associated with wind generation that currently accounts for the majority of renewables can be more of a practical concern for transmission system operation. The change in wind speed and direction may cause significant variability in the generation. Also, a number of utility-scale wind farms are often built along a wind corridor taking advantage of the relatively steady wind speed. This may also cause concurrent variation in wind generation for the sudden change of wind speed or direction, which has been observed from a BNL internal study using wind generation data from ERCOT [Yue 2018]. Such disturbances, coupled with the reduced inertia, will have significant impact on frequency response [Wan 2011] and have to be included in the ESS sizing study. We captured the major uncertainties related to renewables by considering the variability and intermittency of wind generation.

In addition, the net load curves or “duck curves” may change from year to year, mainly due to the increasing renewable generation in the grid. After the ESS sizing is done, a recurrent assessment of the grid inertial responses would be needed. This has also been performed in this study. A method has been developed to tune parameters for solar/wind disturbance models to reflect the changes in overall net load curve.

Stochastic Operation of ESSs

Once ESSs are deployed, the next important question is to efficiently operate ESSs together with other generating units. Uncertainties of particular concern include generation uncertainties in the transmission grid (e.g., large solar or wind farms), the increasing load uncertainties because of behind-the-meter renewables (e.g., rooftop PVs), the switching between charge and discharge cycles of ESSs, dynamic pricing signals from electricity markets, etc. The optimized operation of ESSs was formulated within the context of stochastic unit commitment and economic dispatch with constraints on ESS operation requirements such as depth-of-discharge and state-of-charge, etc. The problem was converted to an MILP problem.

Overview of Methodology Development

There are many studies on ESS sizing and operation based on stochastic optimization. However, the existing solutions usually are applicable to relatively small systems and cannot be scaled up to utility-scale systems, especially when the complexity is drastically increased due to the consideration of frequency dynamics constraints. A probabilistic approach for sizing Battery Energy Storage Systems (BESSs) was presented in [Yue 2015]. The major feature of this approach is that it captures uncertainties of major credible disturbances and explicitly evaluates the grid inertial responses to such disturbances. Although such an approach is extensible to account for disturbances associated with wind generation, the study focused only on the technical performance with and without ESSs, not the associated costs.

ESS planning and operation parts of the study share similar methodologies. Both are formulated as stochastic optimization problems based on a mathematical model of the power system and stochastic models of for renewable generation mainly wind power at the transmission level. Specifically, the stochastic models are incorporated into a unit commitment model similar to those used in industry on a daily basis. More importantly, to ensure that there is adequate grid inertia such that the system frequency is maintained at safe levels, three frequency dynamics constraints, i.e., Frequency nadir (FN), Rate-of-change-of-frequency (RoCoF), and Quasi-steady-state (QSS) are considered in the optimization models. The problems were converted to Mixed-Integer Linear Programming (MILP) problems.

Unit commitment problems are generally difficult to solve because of the existence of discrete decision variables. To address its complexity, and in particular, the complexity brought by the ESSs and the three frequency dynamic constraints, a deterministic model was first considered for the operation problems. A novel decomposition and coordination method based on the Surrogate Absolute-Value Lagrangian Relaxation (SAVLR) [Bragin 2019, Luh 2020], a state-of-the-art dual method, is developed. In the method, a proper direction to update multipliers is obtained without optimally solving all subproblems, resulting in much reduced computational requirements and much less zigzagging of multipliers. Also, convergence to the multiplier optimum does not require the knowledge of the optimal dual value or their estimates. The method has also been synergistically integrated with branch-and-cut, allowing exploitation of both separability and linearity. To improve performance, constraints are also tightened in a systematic way [Yan 2020]. For the deterministic ESS model with the three frequency dynamics constraints, excellent testing results have been obtained for the large Polish system [MATPOWER].

In this study, the major uncertainty source considered is from the utility-scale wind farm generation. In the ESS planning problem formulation, uncertainties are modeled by using a random field theory (RFT) based approach. The goal is to appropriately size ESSs such that the frequency dynamics requirements (FN, RoCoF, and QSS) are satisfied under various scenarios. To consider uncertainties in the ESS operation problems, the uncertain wind generation is modeled as a discrete Markov process considering spatial-temporal correlation of wind speeds among multiple windfarms. Here, the goal is to minimize the total operation costs with given ESS capacities, while considering the Markovian wind generation model and frequency dynamics constraints. The possible wind generation states at windfarms and their probabilities of occurrence are efficiently calculated in the preprocessing stage. To reduce computational requirements caused by the Markov process, the ordinal-optimization concept is introduced where subproblems are approximately solved by using much simplified Markov models subject to the “Surrogate Optimality Condition” with much reduced complexity.

Battery energy storage systems (BESSs) are considered in this study due to their popularity. However, the developed methodology and the tools can be used for ESSs of any technologies.

Contributions

The major contributions of this study include:

- i. Development of the Markovian approach-based model and RFT-based approach for a more realistic representation of wind generation related uncertainties that are suitable for ESS operation and planning studies by considering both spatial and temporal evolutions of wind speed information
- ii. Performance of a systematic constraint tightening approach that may significantly reduce the computational requirements to solve MILP problems
- iii. Refinement of a scalable Surrogate Absolute-Value Lagrangian Relaxation method that can be easily scaled up for large systems via a decomposition and coordination approach
- iv. Development of a rolling horizon-based concept that can be used together with the SAVLR to create the “SAVLRseq” approach that enables practical solutions to long-term planning problems without requiring high performance computing (HPC) facilities.
- v. Introduction of an ordinal-optimization (OO) concept to approximately solve a Markovian subproblem in ESS operation via simplified models with much reduced complexity while maintaining the quality of the overall solution

- vi. Implementation of the SAVLR and SAVLRseq in an open-source, modular, and flexible tool that is readily used for solving utility-scale UC problems.
- vii. An initiation of the development of an innovative integrated mathematical optimization and machine learning (ML) method, i.e., a ML-assisted SAVLR or ML-SAVLR, to address the complexity of the optimal planning and operation.

Conclusions and Insights:

The methodology and the tools developed in this project have been successfully applied to perform frequency dynamics constrained ESS sizing and operation using two example systems, i.e., the IEEE 118-bus system and the 2,283-bus Polish system. ESSs are demonstrated to provide valuable grid inertia support, and, to a lesser extent, peak shaving and reserve services to improve the economic efficiency of grid operation.

A number of conclusions and insights has been achieved in the study:

- i. Responsive ESSs play a critical role in improving the stability and reliability by providing frequency support in low inertia conditions, especially under intermittent wind generation.
- ii. Without deployment of ESSs, load shedding may be unavoidable due to intermittency when the penetration level of the wind generation is high, even without generator outages. This is mainly because of the insufficient fast generation for provisioning the frequency support.
- iii. Realistic uncertainty modeling must be performed by not only considering the spatial and temporal correlations of environmental conditions such as wind speed, precipitation, solar irradiance, temperature, but also the trend of the variations in these conditions. The RFT-based and the Markovian approaches are capable of capturing the correlations and trend of the weather conditions and the renewable generation profiles.
- iv. When considering the frequency constraints including frequency nadir, rate of change of frequency, and quasi-steady-state frequency responses, the complexity of the UC-based ESS planning and operation problems increases tremendously.
- v. Solving the frequency dynamics constrained UC problems for ESS planning and operation is beyond the capability of the existing stochastic optimization methods except the SAVLR and SAVLRseq developed in this study.

Future Work

Additional studies are identified and presented here.

- i. Popular battery technology-based energy storage systems are considered in this study. The methodology and the tools developed can be further extended to evaluate ESSs of different technologies such as flywheel, pump hydro, supercapacitor.
- ii. The frequency constraints related to frequency nadir, RoCoF, and QSS were derived based aggregated system wind equations and are actually conservative, which leads to conservativeness in the investment and installation of ESS capacities. This can be further investigated and improved in the future studies.
- iii. The ESS planning and operation studies can be investigated by further considering the solar generation as well as the possible correlation between wind and solar resources.
- iv. The SAVLR and SAVLRseq tools can be further tested by applying to the planning and operation of ISO-scale systems.

- v. The ML-assisted SAVLR method will be continually developed and further enhanced by developing a distributed and asynchronous version and extending the theoretical results from centralized coordination to distributed coordination while aiming at large-scale implementation.

It should also be noted that the methodology and tool developed are not limited to ESS planning and operation problems. They can also be tailored and used for solving generic stochastic optimization problems. The study in this project is an important step for economically and reliably accommodating more renewable generation via the assistance of ESSs while maintaining stability of the grid dynamics under various disturbances and uncertainties.

1. Introduction

Grid inertia provided by conventional generators plays a vital role in maintaining the system dynamic responses and suppressing disturbances that originate both within and outside of the grid. The rapidly increasing penetration of intermittent renewables such as solar and wind causes a rising concern with the performance of grid frequency response, especially under light load conditions. Large power mismatches caused by high fluctuations of renewables may further exacerbate grid inertial responses. Loss of inertia is thus a grave concern to grid operators. A possible means to achieve a healthy dynamic response is to make use of the responsive energy storage systems (ESSs). ESSs possess response speeds that are superior to conventional generators and can significantly improve grid inertia responses. In addition, ESSs are beneficial to operations by providing much needed energy, ramping as well as reserve services, especially under high penetration of intermittent renewables.

While the effectiveness of the ESS response is well-known, the major challenges that need to be addressed before ESS deployment are (1) what are the required capacities of ESSs, i.e., the sizing of ESSs, to achieve desired inertial responses to different types of disturbances; and (2) how to efficiently operate the grid with ESSs to ensure efficiency, security, and reliability, upon their deployment. The major purpose of this proposal is to develop revolutionary methodologies to answer these questions.

To answer the questions above, the study consists of two closely connected topics, i.e., probabilistic sizing of ESSs based on grid-inertia responses under high penetration of renewables; and stochastic operation optimization of ESSs accounting for the intermittence of renewable generation and the increasing load uncertainties because of behind-the-meter renewables (e.g., rooftop PVs). The grid dynamic response-based ESS sizing ensures the frequency stability, while stochastic operation optimization ensures efficiently and reliably running of ESSs together with other units on the grid, under credible disturbances and increasing uncertainties with renewables.

Probabilistic Sizing of ESSs Considering Variability of Renewables

There are many challenges that impact the grid security and reliability. It is neither impossible nor necessary (affordable) to plan for the worse case scenarios. Rather, we should consider the consequence of the undesired events as well as the probabilities of the occurrences of such events. Therefore, it is preferred to adopt a probabilistic approach to sizing ESSs in a system, and uncertainty modeling becomes an important part of the study.

The uncertainties associated with wind generation that currently accounts for the majority of renewables can be more of a practical concern for transmission system operation. The change in wind speed and direction may cause significant variability in the generation. Also, a number of utility-scale wind farms are often built along a wind corridor taking advantage of the relatively steady wind speed. This may also cause concurrent variation in wind generation for the sudden change of wind speed or direction, which has been observed from a BNL internal study using wind generation data from ERCOT [Yue 2018]. Such disturbances, coupled with the reduced inertia, will have significant impact on frequency response [Wan 2011] and have to be included in the ESS sizing study. We captured the major uncertainties related to renewables by considering the variability and intermittency of wind generation.

In addition, the net load curves or “duck curves” may change from year to year, mainly due to the increasing renewable generation in the grid. After the ESS sizing is done, a recurrent assessment of the grid inertial responses would be needed. This has also been performed in this study. A method has been

developed to tune parameters for solar/wind disturbance models to reflect the changes in overall net load curve.

Stochastic Operation of ESSs Considering Intermittent Renewable Generation and Increasing Load Forecasting Uncertainties

Once ESSs are deployed, the next important question is to efficiently operate ESSs together with other generating units. Uncertainties of particular concern include generation uncertainties in the transmission grid (e.g., large solar or wind farms), the increasing load uncertainties because of behind-the-meter renewables (e.g., rooftop PVs), the switching between charge and discharge cycles of ESSs, dynamic pricing signals from electricity markets, etc. The optimized operation of ESSs was formulated within the context of stochastic unit commitment and economic dispatch with constraints on ESS operation requirements such as depth-of-discharge and state-of-charge, etc. The problem was converted to an MILP problem.

Overview of Methodology Development

There are many studies on ESS sizing and operation based on stochastic optimization. However, the existing solutions usually are applicable to relatively small systems and cannot be scaled up to utility-scale systems, especially when the complexity is drastically increased due to consideration of frequency dynamics constraints. A probabilistic approach for sizing Battery Energy Storage Systems (BESSs) was presented in [Yue 2015]. The major feature of this approach is that it captures uncertainties of major credible disturbances and explicitly evaluates the grid inertial responses to such disturbances. Although such an approach is extensible to account for disturbances associated with wind generation, the study focused only on the technical performance with and without ESSs, not the associated costs.

ESS planning and operation parts of the study share similar methodologies. Both are formulated as stochastic optimization problems based on a mathematical model of the power system and stochastic models of for renewable generation mainly wind power at transmission level. Specifically, the stochastic models are incorporated into a unit commitment model similar to those used in industry on a daily basis. More importantly, to ensure that there is adequate grid inertia such that the system frequency is maintained at safe levels, three frequency dynamics constraints, i.e., Frequency nadir (FN), Rate-of-change-of-frequency (RoCoF), and Quasi-steady-state (QSS) are considered in the optimization model. The problem was converted to an MILP problem.

Unit commitment problems are generally difficult to solve because of the existence of discrete decision variables. To address its complexity, and in particular, the complexity brought by the ESSs and the three frequency dynamic constraints, a deterministic model was first considered for the operation problems. A novel decomposition and coordination method based on the Surrogate Absolute-Value Lagrangian Relaxation (SAVLR) [Bragin 2019, Luh 2020], a state-of-the-art dual method, is developed. In the method, a proper direction to update multipliers is obtained without optimally solving all subproblems, resulting in much reduced computational requirements and much less zigzagging of multipliers. Also, convergence to the multiplier optimum does not require the knowledge of the optimal dual value or its estimates. The method has also been synergistically integrated with branch-and-cut, allowing exploitation of both separability and linearity. To improve performance, constraints are also tightened in a systematic way. For the deterministic ESS model with the three frequency dynamics constraints, excellent testing results have been obtained for the large Polish system.

In this study, the major uncertainty source considered is from the utility-scale wind farm generation. In the ESS planning problem formulation, uncertainties are modeled by using a random field theory (RFT) based approach. The goal is to appropriately size ESSs such that the frequency dynamics requirements (FN, RoCoF, and QSS) are satisfied under various scenarios. To consider uncertainties in the ESS operation problems, the uncertain wind generation is modeled as a discrete Markov process considering spatial-temporal correlation of wind speeds among multiple windfarms. Here, the goal is to minimize the total operation costs with given ESS capacities, while considering the Markovian wind generation model and frequency dynamics constraints. The possible wind generation states at windfarms and their probabilities of occurrence are efficiently calculated in the preprocessing stage. To reduce computational requirements caused by the Markov process, the ordinal-optimization concept is introduced where subproblems are approximately solved by using much simplified Markov models subject to the “Surrogate Optimality Condition” with much reduced complexity.

Battery energy storage systems (BESSs) are considered in this study due to their popularity. However, the methodology and the tools developed can be used for ESSs of any technologies.

After the introduction section, Section 2 provides an overview of the overall methodology adopted in the project. ESS planning and operation problems are formulated, and the solution strategies are discussed in Sections 3 and 4, respectively, with detailed presentation of RFT-based and Markov model-based uncertainty modeling. The structure of the SAVLR and SAVLRseq tools is delineated in Section 5. Case studies for ESS planning and operation are performed and discussed in detail by using the SAVLR and SAVLRseq tools for an IEEE 118-bus system and a 2,383-bus Polish System. The conclusions and findings are presented in Section 7 of this report.

2. Overview of Methodology Development

2.1 Uncertainty Modeling

The uncertainties and intermittency associated with the renewable generation are the major driver calling for deployment and assistance of energy storage systems. And the uncertainty modeling of the renewables is the major challenge in stochastic optimization-based UC for long-term and operational planning. Renewable generation relies on the environmental conditions such as irradiance, wind speed, temperature etc., which are part of the dynamic climate models and are thus both spatially and temporally correlated.

While the generation of renewables constantly fluctuates all the time, i.e., it evolves temporally, the generation from collocated renewable plants or the plants that are physically close may tend to change in the same manner due to the similar changes in environmental conditions. Figure 1 shows an illustrative example of simultaneous wind generation (normalized) reduction within a very short time period (less than 30 minutes) for two highly correlated wind farms. In Table 1, the percentage of simultaneous generation changes is given for different values of Pearson’s correlation coefficient between two wind farms. The correlations appear to be closed related to the distances between different wind generation sites. Table 1 shows that highly correlated renewable plants are more likely to experience similar generation change concurrently. Therefore, both temporal and spatial correlation of renewable generation have to be fully considered in the planning and operation problems. All of these results were obtained from 5-minute interval historical data from ERCOT.

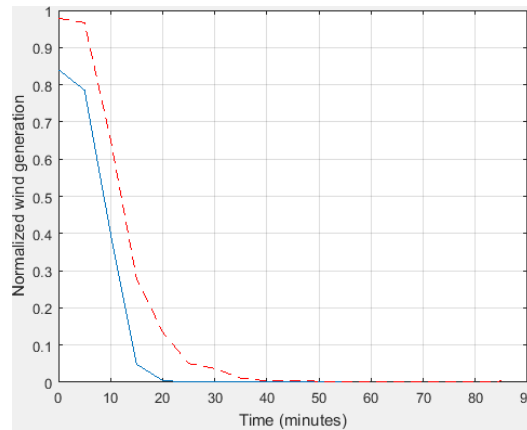


Figure 1: An Example of Concurrent Reduction in Generation of Two Highly Correlated Wind Farms

Table 1: Wind Farm Correlation vs. Percentage of Concurrent Changes in Generation of Two Wind Farms

Pearson’s Correlation between wind farms (i, j)	Percentage of simultaneous under- or over-generation between i and j
0.8 – 1.0	22.6%
0.6 – 0.8	11.2%
0.4 – 0.6	9.6%
0.2 – 0.4	8.7%
0.0 – 0.2	6.1%

The complexity of the climate models prevents the deterministic modeling of such environmental conditions in physics based governing equations. In this study, two modeling approaches are adopted to model the uncertainties and variabilities of the renewable generation, particularly the wind generation, in ESS planning and operation studies. The first approach is based on an analytical model assuming the wind speed field changes follow a Markov process while the second approach is based on a data-driven random field theory. The two approaches are used to model the wind farm generation variations for ESS operation and sizing and siting, respectively, as discussed below.

2.1.1 A Markovian Approach for ESS Operation Studies

Markov processes are widely used to model systems whose states evolve over time with uncertainties. They have the Markov property, i.e., “the future is independent of the past if the present is known.” Thus, these processes are useful for modeling stochastic processes for which the probabilities of states at the subsequent time step can be accurately modelled based on states at the present without the need to consider past states, thus significantly reducing the memory requirements. Markov processes have been shown to effectively model natural phenomenon such as wind speed.

In this study, the wind speeds at wind farms at multiple locations are modeled as a Markov chain (a discrete-time and discrete-state Markov process) with consideration of spatio-temporal correlations between the multiple sites. Once wind speed states are obtained, they are mapped to wind generation states based on the non-linear wind speed to power curve of the windfarms.

2.1.2 Random Field Approach for ESS Planning Studies

While the Markovian approach can be used to model the wind generation evolution efficiently, the number of states will increase exponentially as the number of transitions increases. For the long-term planning problems, the size of the Markov model becomes quickly intractable and an alternative way of uncertainty modeling for the wind generation needs to be developed.

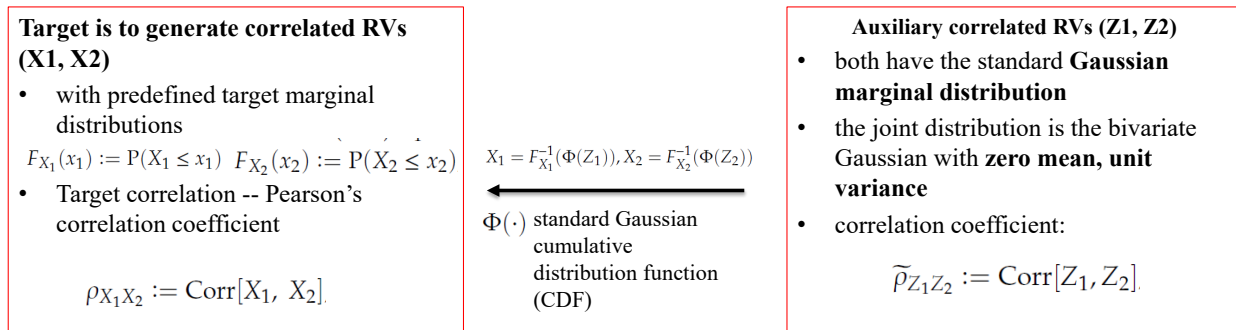
A random field (RF) is a generalization of a stochastic process while the underlying parameter does not have to be real or integer valued "time" but can instead take values that are multidimensional vectors or points on some manifolds [Vanmar 2010]. The word “field” implies that the geometric structure of the parameter space is emphasized. Random field theory (RFT) provides a very appropriate way of modeling the processes that evolve in both time and space such as wind speed and solar irradiance across a large area/various locations.

Gaussian and Gaussian-related random field refers to a random field f on a parameter set T for which the distributions vector valued random variables $(f_{t_1}, f_{t_2}, \dots, f_{t_n})$ are multivariate Gaussian. For such random fields, the first order and second order properties (i.e., mean, variance, and covariance) of the random variables (RVs) are insufficient to describe them. In reality, there are barely any processes that fit a Gaussian distribution. To consider non-Gaussian option, a non-Gaussian process may (1) be decomposed into and approximated by a mixture of Gaussian models and (2) follow specific processes, such as χ^2 or t -Student, Gamma, or skew normal distributions. These approaches, however, are not flexible enough to model complex processes when these processes are intermittent, and the continuous part of their marginal distribution is characterized by large variability in shape [Papale 2019]. Distributions such as the Gamma and the Exponential distributions have thin tails and cannot model adequately extremes of heavy-tailed variables such as wind speed.

In this study, we adopted a framework suitable for simulating random field representation of climate variables, which are non-Gaussian, intermittent, dependent, and periodic, of a desired marginal probability distribution (including mixed-type and discrete marginals) and spatiotemporal correlation structure. This framework is closely related to a so-called Nataf’s joint distribution model or NDM. Based on the NDM and the inverse cumulative distribution functions (ICDFs), an auxiliary multivariate standard Gaussian distribution can be mapped to obtain the joint distribution of random variables with any target arbitrary marginal distributions. The link between correlation coefficients in the Gaussian and the target domain RVs is used to also reproduce the target correlations.

Figure 2 shows a case for bivariate random field, i.e., the joint distribution of two RVs is developed using the target marginal distribution(s) and correlations to first generate the joint distribution for the auxiliary correlated Gaussian RVs (in the right side of Figure 2) and then convert the joint distribution for Gaussian RVs using the ICDF. The target marginal distribution(s) and correlation(s) can be obtained based on historical measurements. Note that, the auxiliary Gaussian process with zero mean and unit variance is simulated via linear stochastic models such as an autoregressive moving average (ARMA) models) to capture the temporal correlation of each random variable.

Such a concept is adopted in an open-source simulation software anySim [Tsouka 2020], which is used in this study to simulate the wind speed, based on the historical information. The simulated wind speed data is later converted to time-series wind generation data.



$F_{X_1}^{-1}(\cdot)$ and $F_{X_2}^{-1}(\cdot)$ denote the inverse cumulative distribution functions (ICDF)

Figure 2: The NDM for bivariate random field.

2.2 Constraint Tightening

A systematic approach was recently developed to tighten unit commitment in MILP formulations (actually Mixed-Binary Linear Programming formulations) [Yan 2020]. For an MILP problem, if the constraints directly delineate its convex hull, i.e., the formulation is “tight,” then the problem can be directly solved by using linear programming methods without combinatorial difficulties. In our approach, tightened constraints are established based on a novel integration of “constraint-and-vertex conversion,” “vertex elimination” and “parameterization.” For a unit with given set of parameters, the integrality requirements are relaxed, and vertices of constraints are generated. The vertices with fractional values for binary variables are eliminated. The remaining vertices are proved to be the vertices of the convex hull to the original MILP problem. These vertices are converted back to constraints, which are tight and are then parameterized in terms of original unit parameters for general use. For practical applications, “near-tight” formulations are obtained by analyzing short-time horizon problems, e.g., three hours, with tremendous

reduction of online computational requirements. In this project, the near-tight formulation of [Yan 2020] is used as the basis of the deterministic UC model.

2.3 SAVLR with Soft Constraints

As reviewed in Section 1, the SAVLR is a recently developed, state-of-the-art dual method. It is applicable to non-separable problems, because subproblems can still be formed and solved within its framework as long as their solutions satisfy the “Surrogate optimality condition.” This allows for the innovative exploitation of “soft” constraints – constraints that do not need to be strictly satisfied but their violations are penalized by predetermined coefficients. In this project, by not relaxing the majority of coupling constraints but treating them as soft, the number of multipliers is significantly reduced while coordination with respect to the unrelaxed constraints is facilitated by exploiting their “softness,” leading to faster convergence and improved solution quality. See Figure 3 for a flowchart of the SAVLR.

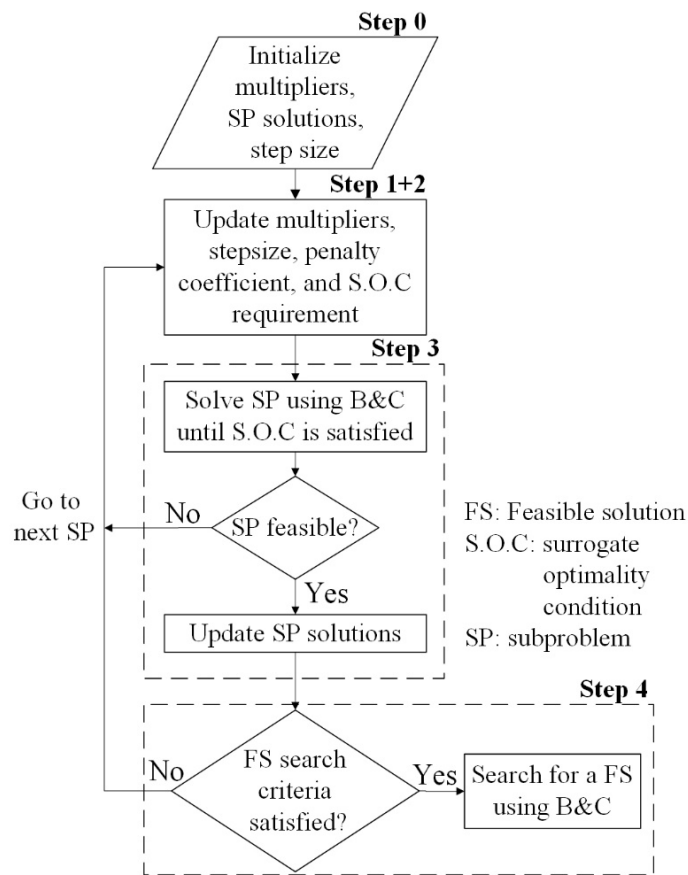


Figure 3: Flowchart of SAVLR

All of the techniques have been combined and implemented to solve the ESS planning and operation studies, as discussed in the next two sections.

3. ESS Planning Study

3.1 Problem Formulation

The ESS planning is modeled as a stochastic programming problem with uncertainties represented by different scenarios. The investment for deploying ESSs of an appropriate capacity, is a here-and-now variable while the conventional generators' output and ESS charging/discharging power are the wait-and-see variables. In the problem formulation, we use a random field theory (RTF) approach to model the correlated wind power generation from different wind farms in the power grid. For each scenario representing a snapshot of the system operating condition, the unit commitment is then performed to determine the on/off status of generators. The details of the ESS planning problem are given below.

3.1.1. Objective Function

The objective function given in (1) consists of investment cost of ESS and the operation cost including the expenses for operating conventional generation, load shedding, and renewable shedding. The BP_i^{ch} and BP_i^{dch} are set to be equal to BE_i .

$$\min \sum_{i \in \Omega_E} c_i^E BE_i + \sum_{\omega} p_{\omega} \sum_t (\sum_{i \in \Omega_G} (c_i^g P g_{it}^{\omega} + c_i^{SU} S U_{it}^{\omega} + c_i^{NL} u_{it}^{\omega}) + \sum_{i \in \Omega_B} c_i^{ls} P d_{it}^{s\omega} + \sum_{i \in \Omega_W} c_i^{rs} P r_{it}^{s\omega}) \quad (1)$$

3.1.2. System Constraints

The objective function is optimized while satisfying the DC power flow constraints, which include the nodal power balance (2) and branch power balance (3) [Zhan 2019]. The nodal power balance (2) considers the conventional generation, ESS, renewable generation/curtailment, the load demand/shedding, and branch power flow. Eq. (4) indicates branch capacity lower and upper limits. Eq. (5) is the generation limit based on its on/off status. In the equations, hereafter, $\forall \omega \in \Omega_{\omega}$ and $\forall t \in \Omega_T$ hold unless otherwise stated.

$$\sum_{y \in i} P g_{yt}^{\omega} - P b_{it}^{c,\omega} + P b_{it}^{d,\omega} + P r_{it}^{o\omega} - P r_{it}^{s\omega} + P d_{it}^{s\omega} - P d_{it}^{\omega} = \sum f_{ijt}^{\omega}, \quad \forall i \quad (2)$$

$$f_{ijt}^{\omega} = (\theta_{it}^{\omega} - \theta_{jt}^{\omega}) / X_{ij}, \quad \forall ij \quad (3)$$

$$\underline{f}_{ij} \leq f_{ijt}^{\omega} \leq \bar{f}_{ij}, \quad \forall ij \quad (4)$$

$$u_{it}^{\omega} \underline{P} g_i \leq P g_{it}^{\omega} \leq u_{it}^{\omega} \bar{P} g_i, \quad \forall i \in \Omega_G \quad (5)$$

Eq. (6) represents the change of battery state of charge (SoC) between two consecutive hours. Eq. (7) denotes the allowable lower and upper bounds of SoC. Eq. (8) requires that the SoC in the beginning and ending moments of a time horizon is the same such that different scenarios are independent. Note that SoC represents energy to avoid bilinear terms in the model.

$$SOC_{i,t}^{\omega} = SOC_{i,t-1}^{\omega} + \eta_i^{ch} P b_{it}^{c,\omega} \Delta t - P b_{it}^{d,\omega} \Delta t / \eta_i^{dch}, \quad \forall i \in \Omega_E \quad (6)$$

$$0.3 * BE_i \leq SOC_{i,t}^{\omega} \leq BE_i, \quad \forall i \in \Omega_E \quad (7)$$

$$SOC_{i,n_t}^{\omega} = SOC_{i,0}^{\omega} = 0.5 BE_i, \quad \forall i \in \Omega_E, \quad (8)$$

Eqs. (9) represents the spinning reserve. Due to its fast response, ESS can quickly switch from charging or partly discharging mode to the fully discharging mode, which is utilized as a spinning reserve in (9). The value $SOC_{i,t}^{\omega} / \Delta t$ represents the available discharging power for the whole duration Δt . The system reserve can be set to the capacity of the largest unit in the system or a fixed percentage of the system load. Eq. (10)/(11) represents the lower and upper bounds of ESS charging/discharging power. Eq. (12)

assures that charging and discharging do not occur simultaneously. Eqs. (13) and (14) guarantee the minimum up- and down-time of conventional generators, respectively. Eq. (15) models the startup or shutdown logic. Eqs. (16) and (17) maintain the limits of ramp-rate up and down, respectively.

$$\sum_{i \in \Omega_G} (u_{it}^\omega \overline{Pg}_i) + \sum_{i \in \Omega_E} (Pb_{it}^{c,\omega} + SOC_{i,t}^\omega / \Delta t - Pb_{it}^{d,\omega}) + \sum_{i \in \Omega_W} (Pr_{it}^{\omega} - Pr_{it}^{s\omega}) + \sum_{i \in \Omega_B} (Pd_{it}^{s\omega} - Pd_{it}^\omega) \geq R_t^\omega \quad (9)$$

$$0 \leq Pb_{it}^{c,\omega} \leq \alpha_{it} BP_i^{ch}, \quad \forall i \in \Omega_E \quad (9)$$

$$0 \leq Pb_{it}^{d,\omega} \leq \beta_{it} BP_i^{dch}, \quad \forall i \in \Omega_E \quad (10)$$

$$\alpha_{it} + \beta_{it} \leq 1, \quad \forall i \in \Omega_E \quad (11)$$

$$\sum_{y=t-\tau_i^+}^t SU_{iy}^\omega \leq u_{it}^\omega, \quad \forall i \in \Omega_G \quad (12)$$

$$\sum_{y=t-\tau_i^-}^t SD_{iy}^\omega \leq u_{it}^\omega, \quad \forall i \in \Omega_G \quad (13)$$

$$u_{it}^\omega - u_{i(t-1)}^\omega = SU_{it}^\omega - SD_{it}^\omega, \quad \forall i \in \Omega_G \quad (14)$$

$$Pg_{it}^\omega - Pg_{i,t-1}^\omega \leq RU_i, \quad t = 2, 3, \dots, n_t, \forall i \in \Omega_G \quad (15)$$

$$Pg_{i,t-1}^\omega - Pg_{it}^\omega \leq RD_i, \quad t = 2, 3, \dots, n_t, \forall i \in \Omega_G \quad (16)$$

3.1.3. Frequency Dynamics Security Under Contingencies

3.1.3.1 Rate of Change of Frequency (RoCoF)

Eq. (18) represents the system inertia in contingency κ , which includes the inertia from online generators and the emulated inertia from wind turbines. Note that $\forall \kappa \in \Omega_\kappa$ holds for (18)-(31), (39), and (42) but not specifically written out.

$$H_t^{\omega\kappa} = (\sum_{i \in \Omega_G \setminus \Omega_\kappa} u_{it}^\omega \overline{Pg}_i H_i + \sum_{i \in \Omega_W \setminus \Omega_\kappa} (Pr_{it}^{\omega} - Pr_{it}^{s\omega}) H_i) / f_0, \quad (17)$$

Eqs. (19) and (20) guarantee the system inertia after contingency κ is large enough such that the RoCoF is not violated. Eq. (19) is related to insufficient generation ($\Delta g_{t,u}^{\omega\kappa}$) while (20) is related to excess generation ($\Delta g_{t,o}^{\omega\kappa}$) caused by upward wind power fluctuation.

$$H_t^{\omega\kappa} 2RoCoF^{\max} \geq \Delta g_{t,u}^{\omega\kappa}, \quad (19)$$

$$H_t^{\omega\kappa} 2RoCoF^{\max} \geq \Delta g_{t,o}^{\omega\kappa}, \quad (20)$$

After contingency κ , the insufficient generation ($\Delta g_{t,u}^{\omega\kappa}$) in the system is defined in (21), where the four terms on the right-hand side are the total power output of lost generators, decreased wind power output due to its fluctuation, and the increased power output from ESSs, respectively. The excess generation ($\Delta g_{t,o}^{\omega\kappa}$) in the system is defined in (22) and can be similarly explained. The wind power fluctuations (represented by) wd_{it}^ω and wu_{it}^ω are used to represent the decrease and increase fluctuation, respectively.

$$\Delta g_{t,u}^{\omega\kappa} = \sum_{i \in \Omega_\kappa} Pg_{it}^\omega + \sum_{i \in \Omega_\kappa} (wd_{it}^\omega - wu_{it}^\omega) - Pb_{d,t}^{\omega\kappa}, \quad \Delta g_{t,u}^{\omega\kappa} \geq 0, \quad (18)$$

$$\Delta g_{t,o}^{\omega\kappa} = -\sum_{i \in \Omega_\kappa} Pg_{it}^\omega + \sum_{i \in \Omega_\kappa} (-wd_{it}^\omega + wu_{it}^\omega) - Pb_{c,t}^{\omega\kappa}, \quad \Delta g_{t,o}^{\omega\kappa} \geq 0, \quad (19)$$

The increased power output comes from the battery, and the maximum output can be increased, as given on the right-hand side of (23). If the battery is operating in the charging mode, $b_{it}^{d,\omega} = 0$, it contributes $Pb_{it}^{c,\omega} + BP_i^{dch}$ to the increased power. If the battery is operating in the discharging mode, $b_{it}^{c,\omega} = 0$, it

contributes $BP_i^{dch} - Pb_{it}^{d,\omega}$ to the increased power, i.e., the battery increases its discharging power to its maximum value. The decreased power output from the battery is modeled in (24) and can be similarly explained.

$$Pb_{d,t}^{\omega\kappa} \leq \sum_{i \in \Omega_E} (Pb_{it}^{c,\omega} + BP_i^{dch} - Pb_{it}^{d,\omega}), \quad (20)$$

$$Pb_{c,t}^{\omega\kappa} \leq \sum_{i \in \Omega_E} (BP_i^{ch} - Pb_{it}^{c,\omega} + Pb_{it}^{d,\omega}), \quad (21)$$

3.1.3.2 Frequency Nadir Constraints

After a contingency, if the total system spinning reserve is smaller than the system power mismatch $\Delta g_{t,u}^{\omega\kappa}$, the mechanical power is always less than the electrical load and, therefore, the system frequency keeps on decreasing according to the frequency dynamics swing equation; and eventually drops below the pre-specified frequency nadir f_{MIN} . Therefore, to maintain the system frequency above nadir, the total system spinning reserve should be larger than the system power mismatch $\Delta g_{t,u}^{\omega\kappa}$, i.e., $\sum_{i \in \{\Omega_G, \Omega_W\} \setminus \Omega_\kappa} g_{it}^{R\omega\kappa} \geq \Delta g_{t,u}^{\omega\kappa}$.

After a contingency, there is a power mismatch between the generation and load, which leads to the instantaneous change of the frequency. This frequency deviation is fed back to generator control, and the rest of the generators try to make up for the lost generation. However, due to the limited ramping capabilities of the conventional generators, the power mismatch remains almost the same during the first second or so (the time frame of inertia response) after the generator outage and the frequency continue to drop until it reaches the nadir. The nadir is almost completely determined by the remaining inertia in the system for the nearly constant power mismatch. Since we cannot change the system inertia, the frequency nadir would be higher if we can reduce the power mismatch. The major role of the ESSs that are very responsive is to decrease the power mismatch in the inertia response process before the rest of the generators pick up the load and restores the frequency dynamics.

The relationship between system ramp up capacity v_{NAD} and frequency nadir f_{MIN} can be expressed as follows [Chavez 2014]:

$$v_{NAD} = \frac{(\Delta g_{t,u}^{\omega\kappa})^2}{2H_t^{\omega\kappa}(f_0 - f_{MIN} - f_{db})} \quad (25)$$

The time to reach the frequency nadir f_{MIN} is the sum of the dead band time and ramp-up time:

$$t_{NAD} = t_d + \Delta g_{t,u}^{\omega\kappa} / v_{NAD} \quad (26)$$

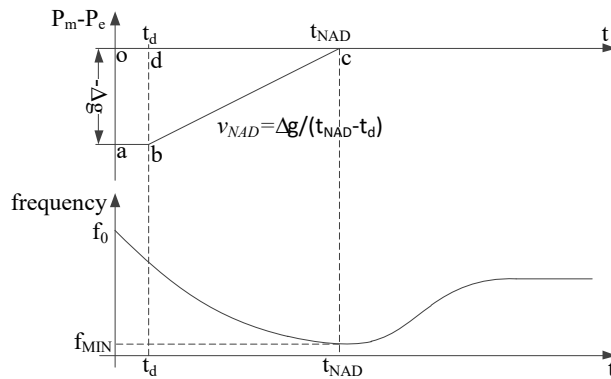


Figure 4. Illustration power mismatch and frequency dynamics.

If the system ramp-up rate is higher (lower) than v_{NAD} , the frequency decelerate area is less (more) than the trapezium area $abco$ in Figure 4; consequently, the value of system frequency nadir is higher (lower) than f_{MIN} . Therefore, in order to avoid system frequency dropping below f_{MIN} , the system ramp-up rate $\sum_{i \in \{\Omega_G, \Omega_W\} \setminus \Omega_\kappa} v_i$ should be larger than or equal to v_{NAD} , i.e.,

$$\sum_{i \in \{\Omega_G, \Omega_W\} \setminus \Omega_\kappa} v_i \geq \frac{(\Delta g_{t,u}^{\omega\kappa})^2}{2H_t^{\omega\kappa}(f_0 - f_{MIN} - f_{db})} \quad (27)$$

which can be reformed to Eq. (28), ensuring enough system inertia and ramp-up capability to maintain frequency **nadir** above the pre-specified value f_{MIN} .

$$2H_t^{\omega\kappa}(f_0 - f_{MIN} - f_{db}) \sum_{i \in \{\Omega_G, \Omega_W\} \setminus \Omega_\kappa} u_{it}^\omega v_i \geq (Pg_{t,u}^{\omega\kappa})^2 \quad (22)$$

Eq. (29) ensures the total spinning reserve is properly allocated to each generator according to its ramp rate capacity

$$0 \leq Pg_{it}^{R\omega\kappa} \leq \frac{u_{it}^\omega v_i}{\sum_{i \in \{\Omega_G, \Omega_W\} \setminus \Omega_\kappa} u_{it}^\omega v_i} \Delta g_{t,u}^{\omega\kappa}, \forall \kappa, \forall i \in \{\Omega_G, \Omega_W\} \setminus \Omega_\kappa \quad (29)$$

According to (25)-(27), $\sum_{i \in \{\Omega_G, \Omega_W\} \setminus \Omega_\kappa} v_i \geq v_{NAD}$, $\Delta g_{t,u}^{\omega\kappa} / v_{NAD} = t_{NAD} - t_d$. Therefore, we have

$$Pg_{it}^{R\omega\kappa} \leq \frac{u_{it}^\omega v_i}{\sum_{i \in \{\Omega_G, \Omega_W\} \setminus \Omega_\kappa} v_i} \Delta g_{t,u}^{\omega\kappa} \leq \frac{u_{it}^\omega v_i}{v_{NAD}} \Delta g_{t,u}^{\omega\kappa} = u_{it}^\omega v_i (t_{NAD} - t_d)$$

That is, $Pg_{it}^{R\omega\kappa} \leq u_{it}^\omega v_i (t_{NAD} - t_d)$, which means that generator i 's ramp up rate is high enough such that it can increase its output by at least $Pg_{it}^{R\omega\kappa}$ within $(t_{NAD} - t_d)$.

In addition, Eq. (30) ensures that the total system spinning reserve, from both conventional generation and wind power, can fully compensate for the power mismatch due to the contingency. Eq. (31) represents that the sum of generation and spinning reserve of a conventional generator should not exceed its online capacity. The available wind power output is not controllable. However, a wind farm can provide reserve if it operates at a de-rated mode, i.e., a part of the available wind power is shed. When a contingency occurs, and more power is needed, the wind farm can increase its output by up to the shed wind power. This reserve from the wind power should not exceed the shed wind power, as modeled in (32).

$$\sum_{i \in \{\Omega_G, \Omega_W\} \setminus \Omega_\kappa} Pg_{it}^{R\omega\kappa} \geq \Delta g_{t,u}^{\omega\kappa}, \quad (30)$$

$$0 \leq Pg_{it}^\omega + Pg_{it}^{R\omega\kappa} \leq u_{it}^\omega \bar{g}_i, \quad \forall i \in \Omega_G \setminus \Omega_\kappa \quad (31)$$

$$Pg_{it}^{R\omega\kappa} \leq Pr_{it}^{s\omega}, \quad \forall i \in \Omega_W \setminus \Omega_\kappa \quad (23)$$

Note that u_{it}^ω for wind farms (i.e., $i \in \Omega_W$) is always set to 1, i.e., wind farms are always at the 'on' status. Considering wind power shedding is used, the wind power connected to the power grid can also be zero equivalent to the 'off' status. This is why u_{it}^ω ($i \in \Omega_W$) needs not being set to 0. Note that the frequency nadir is associated with the insufficient generation ($\Delta g_{t,u}^{\omega\kappa}$). When the frequency is higher than the normal value due to excess generation ($\Delta g_{t,o}^{\omega\kappa}$) is not considered in this model as it can be easily handled by reducing the generation output.

3.1.3.3 Quasi-steady-state Frequency Constraints

Eqs. (33) and (34) maintain the quasi-steady-state frequency within a pre-specified range in all contingencies, which is known as primary frequency regulation. The droop constant DR_i is set to 5%. For

every 1% change in the turbine speed reference, the power output of the turbine changes by 20% of rate for a unit with a 5% droop setting.

$$\frac{\Delta g_{t,u}^{\omega\kappa}}{\Delta f_{qss}^{\omega\kappa}} = \sum_{i \in \{\Omega_G, \Omega_W\} \setminus \Omega_\kappa} \frac{u_{it}^{\omega} \overline{P} g_i}{DR_{if}^0}, \quad (24)$$

$$\Delta f_{qss}^{\omega\kappa} \leq \Delta f_{qss}^{max}, \quad (25)$$

The ESS energy used for IR and PFR should be less than the remaining ESS energy as modeled in (35).

$$P b_{it}^{d,\omega} (\Delta t_{IR} + \Delta t_{PFR}) \leq SOC_{it}^{\omega} \quad (35)$$

3.1.4. Model Linearization

Let $S_{it}^{ch} = \alpha_{it} B P_i^{ch}$ and $S_{it}^{dch} = \beta_{it} B P_i^{dch}$ and then we have

$$0 \leq b_{it}^{c,\omega} \leq S_{it}^{ch} \quad (36)$$

$$0 \leq b_{it}^{d,\omega} \leq S_{it}^{dch} \quad (37)$$

$$0 \leq S_{it}^{ch} \leq \alpha_{it} B P_i^{ch,max} \quad (38)$$

$$B P_i^{ch} - (1 - \alpha_{it}) B P_i^{ch,max} \leq S_{it}^{ch} \leq B P_i^{ch} \quad (39)$$

$$0 \leq S_{it}^{dch} \leq \beta_{it} B P_i^{dch,max} \quad (40)$$

$$B P_i^{dch} - (1 - \beta_{it}) B P_i^{dch,max} \leq S_{it}^{dch} \leq B P_i^{dch} \quad (41)$$

where $B P_i^{ch,max}$ and $B P_i^{dch,max}$ are the upper bounds of $B P_i^{ch}$ and $B P_i^{dch}$, respectively. The right-hand side of (28) has a bilinear term, and (28) can be linearized as:

$$2H_t^{\omega\kappa} (f_0 - f_{MIN} - f_{db}) \sum_{i \in \{\Omega_G, \Omega_W\} \setminus \Omega_\kappa} u_{it}^{\omega} v_i \geq (x_{t,j+1}^{\omega\kappa} + x_{t,j}^{\omega\kappa}) \Delta g_{t,u}^{\omega\kappa} - x_{t,j}^{\omega\kappa} x_{t,j+1}^{\omega\kappa}, \quad \forall j \in \Omega_J, \quad \forall i \in \Omega_G \quad (26)$$

where $x_{t,j}^{\omega\kappa}, \forall j \in \Omega_J = \{0, 1, 2, \dots, n_j\}$ is between the lower and upper bounds of $\Delta g_{t,u}^{\omega\kappa}$ and $x_{t,j+1}^{\omega\kappa} > x_{t,j}^{\omega\kappa}$. Note that $x_{t,j}^{\omega\kappa}$ is a parameter instead of a variable and is simply set to distribute between the lower and upper bounds of $\Delta g_{t,u}^{\omega\kappa}$.

The idea of linearization from Eqs (28) to (42) is explained below. The left-hand side of (28) or (42) has only one variable, i.e., $H_t^{\omega\kappa}$. Let x represent $\Delta g_{t,u}^{\omega\kappa}$. Then, (28) and (42) can be written in a compact form, i.e., $y \geq x^2$ and $y \geq (x_{j+1} + x_j)x - x_{j+1}x_j, \forall j \in \Omega_J$, where x_j are parameters between the lower and upper bounds of $\Delta g_{t,u}^{\omega\kappa}$. In Figure 5, $y \geq x^2$ represents the space on and above the solid line (referred to as space 1), approximated by the space on and above the line segments ABCDEF (referred to as space 2), where the horizontal axis is evenly divided into space five segments by points A-F. Increasing the number of segments can reduce the approximation error of this linearization method.

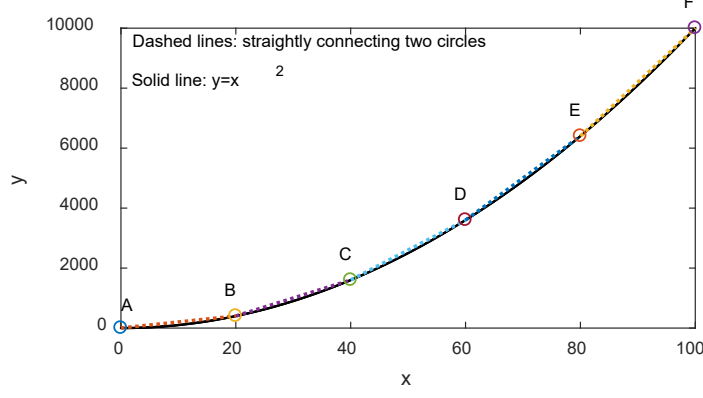


Figure 5. Illustration of linearization of $y \geq x^2$.

Let $y \geq f_{line}(x)$ denote the half-space on and above a straight line. For example, $y \geq f_{Line_{AB}}(x)$ represents the half space on and above a straight $Line_{AB}$ and can be expressed as $y \geq \frac{x_B^2 - x_A^2}{x_B - x_A}x + x_A^2 - \frac{x_B^2 - x_A^2}{x_B - x_A}x_A$, which can be reformed as $y \geq (x_B + x_A)x - x_Ax_B$, where x_A (x_A^2) and x_B (x_B^2) represent the horizontal (vertical) axis value of points A and B, respectively.

As the slope of line segment, BC is deeper than AB, the left-hand side of point B of $Line_{BC}$ is below $Line_{AB}$ and the right-hand side of point B of $Line_{AB}$ is below $Line_{BC}$. After the analogous analysis for each two adjacent line segments of BC, CD, DE, and EF, it can be known that space 2 is exactly the intersection of the five half space on and above $Line_{AB}$, $Line_{BC}$, $Line_{CD}$, $Line_{DE}$, and $Line_{EF}$ in Figure 5, respectively, i.e., space 2 is exactly represented by $y \geq f_{line}(x), \forall line \in \{Line_{AB}, Line_{BC}, Line_{CD}, Line_{DE}, Line_{EF}\}$. Therefore, $y \geq x^2$ can be approximated by $y \geq (x_{j+1} + x_j)x - x_{j+1}x_j, \forall j \in \{0, 1, \dots, 4\}$ where $x_j, j = 0, 1, \dots, 5$, represents x_A, x_B, x_C, x_D, x_E , and x_F , respectively. That is, (28) can be approximated by (42).

The left-hand side of (42) includes a bilinear term, i.e.,

$$H_t^{\omega\kappa} \sum_{i \in \{\Omega_G, \Omega_W\} \setminus \Omega_\kappa} u_{it}^\omega v_i = \frac{1}{f_0} \sum_{i \in \Omega_G \setminus \Omega_\kappa} \sum_{l \in \{\Omega_G, \Omega_W\} \setminus \Omega_\kappa} \overline{Pg}_i H_i (u_{it}^\omega u_{lt}^\omega) v_l + \frac{1}{f_0} \sum_{i \in \Omega_W \setminus \Omega_\kappa} \sum_{l \in \{\Omega_G, \Omega_W\} \setminus \Omega_\kappa} (Pr_{it}^{0\omega} H_i u_{it}^\omega v_l - H_i v_l u_{it}^\omega Pr_{it}^{s\omega})$$

where $u_{it}^\omega r_{it}^{s\omega}$ is the product of binary and continuous variables which can be linearized similar to (36)-(41) and $u_{it}^\omega u_{lt}^\omega$ is a product of two binary variables can be replaced by a new variable uil_{it}^ω subject to the following two constraints:

$$0 \leq uil_{it}^\omega \leq u_{it}^\omega, \quad \forall i \in \{\Omega_G, \Omega_W\}, \forall l \in \{\Omega_G, \Omega_W\} \quad (43)$$

$$u_{it}^\omega + u_{lt}^\omega - 1 \leq uil_{it}^\omega \leq u_{lt}^\omega, \quad \forall i \in \{\Omega_G, \Omega_W\}, \forall l \in \{\Omega_G, \Omega_W\} \quad (44)$$

The u_{it}^ω in the right-hand side of (29) can be dropped and (29) can be replaced by (45). The reason is that if $u_{it}^\omega = 1$, it is obvious that (29) is equivalent to (45). If $u_{it}^\omega = 0$, (31) guarantees that $Pg_{it}^{R\omega\kappa}$ is equal to 0 and both (29) and (45) are relaxed.

$$0 \leq Pg_{it}^{R\omega\kappa} \leq \frac{v_i}{\sum_{i \in \Omega_\kappa} u_{it}^\omega v_i} \Delta g_{t,u}^{\omega\kappa}, \quad \forall i \in \Omega_G \quad (45)$$

Eq. (45) can be rewritten as $g_{it}^{R\omega\kappa} \sum_{i \in \Omega_\kappa} u_{it}^\omega v_i \leq v_i \Delta g_{t,u}^{\omega\kappa}$, the left-hand side of which has a bilinear term, i.e., the product of binary and continuous variables, which can also be linearized similar to (36)-(41).

3.2 Scenario Development

The scenario development here mainly involves in the generation of simulated wind speed data at the wind farm locations that can be used to obtain the future wind generation profile based on the historical wind speed data. One and a half years' 5-minute interval wind speed data at three wind generation sites were obtained from ERCOT. Here, the wind speed at each wind farm is represented by a random variable. A statistic analysis of the wind speed was performed after sanitizing the data. The histograms of original wind speed data for the three wind generation sites are shown in Figure 6. It appears that a normal distribution can be used to fit the histograms well. Based on the assumption of normal distribution, the mean and standard deviation for each distribution were calculated from the original data, as shown in Table 2, where Vw1, ..., Vw3 indicate the wind speed at generation sites 1, ..., 3. The correlations between these three wind generation sites were calculated and are shown in Table 3. Table 3 shows that generation sites 1 and 2 are strongly correlated while their correlations with generation site 3 are relatively weak (see the off-diagonal elements in Table 3).

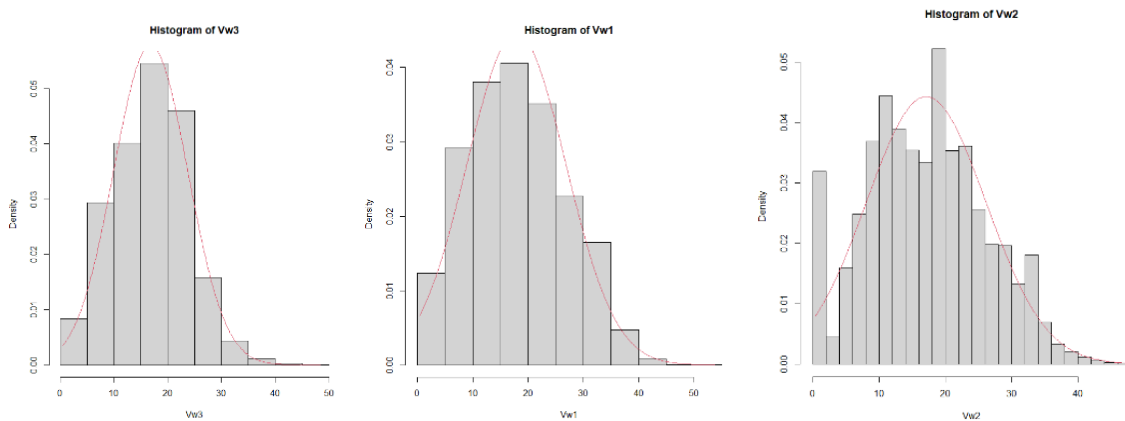


Figure 6: Histogram for wind speed at three wind sites.

Table 2: Mean and standard deviation of historical wind speed data.

Wind sites	Mean	standard deviation
Vw1	17.88443	8.957843
Vw2	17.08378	9.01563
Vw3	16.84704	6.90535

Table 3: The estimated cross-correlation coefficients of the original data.

Wind Sites	Vw1	Vw2	Vw3
Vw1	1.0000	0.82653	0.41758
Vw2	0.82653	1.0000	0.35998
Vw3	0.41758	0.35998	1.00000

As discussed in Section 2.1.2, the target marginal distribution for each of the wind speed is the normal distribution, which is used together with the correlation coefficients as input to anySim tool for deriving the joint distribution of the auxiliary Gaussian RVs. The joint Gaussian distributions are then used to generate the joint distribution for the wind speed via ICDF. Using anySim, we generated one-year wind speed data at the three sites for the future. The simulated wind speed data at three sites are plotted in Figure 7.

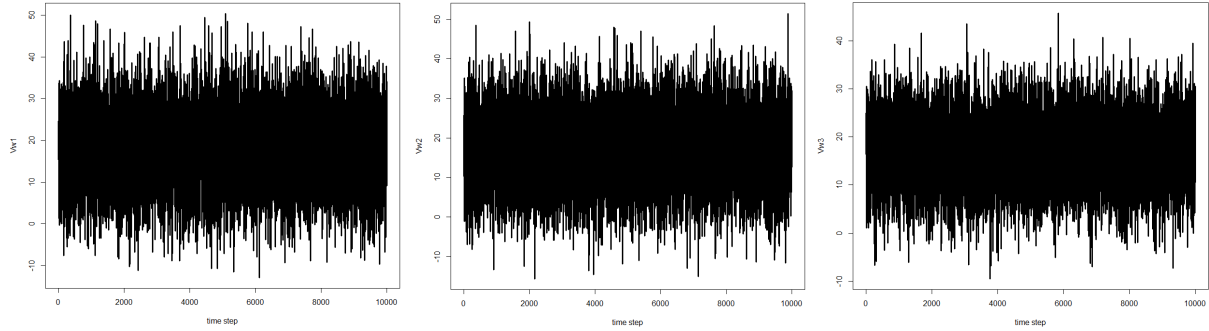


Figure 7: The time series data of the simulation.

To validate that the statistics for the simulated data match those for the original historical data, the histograms (including the mean and deviation of the corresponding normal distribution) and the correlations between them are shown in Figure 8 and Table 4, respectively. It can be seen that both match the properties of the original wind speed data.

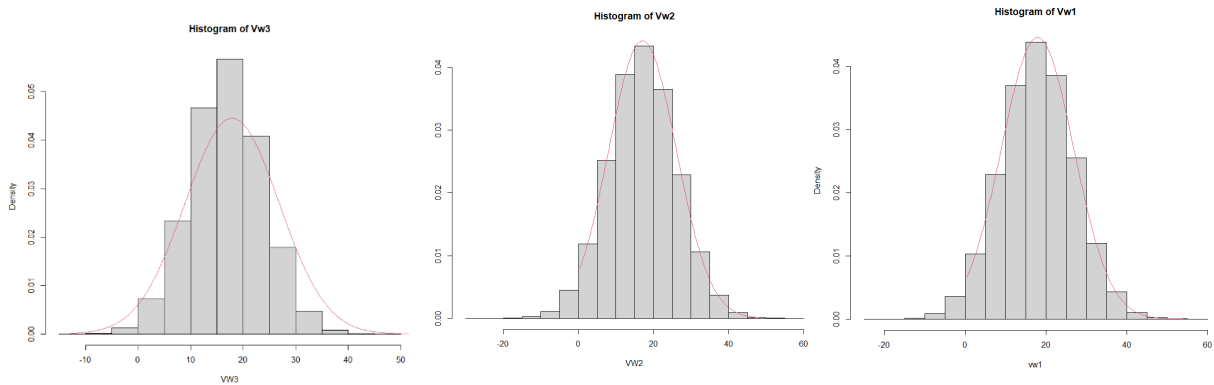


Figure 8: Histograms of simulated data and assumed distribution.

Table 4: The difference between the estimated cross-correlation coefficients of the simulated data and original data (Corr_original – Corr_simul).

Wind Sites	Vw1	Vw2	Vw3
Vw1	0.0000	9.416e-04	-3.652e-03
Vw2	9.416e-04	0.0000	-1.973e-03
Vw3	-3.652e-03	-1.973e-03	0.0000

It should be noted that the RFT-based approach takes advantage of ARMA model and therefore, is able to capture not only the spatial and temporal correlations among various RVs but also the trend of the variations in these RVs. The RFT provides an ideal approach to modeling the variability and correlation of weather related variables such as wind speed, precipitation, solar irradiance, temperature and thus the renewable generation profiles.

3.3 Solutions

The original problem is decoupled into sub-problems following a decomposition and coordination method in the SAVLR introduced in Section 2. To maintain a limited number of multipliers and make the problem complexity applicable, for planning problems, only system demand and frequency nadir constraints are relaxed following the SAVLR framework. Other coupling constraints are converted to soft constraints.

3.3.1. Incorporating Rolling Horizon to SAVLR

The SAVLR method presented above can solve the large-scale operation problems effectively. However, the number of decision variables and constraints would increase significantly with the longer planning horizon, which is always the case in long-term planning, e.g., yearly planning. Although the SAVLR theoretically could still be applied to handle this kind of problems, the real-world limit in computer memory may hinder its application. This is mainly because of the need of the SAVLR to store the initial values for the decision variables and the transmission capacity constraints for all planning scenarios.

Taking the 2,383-bus Polish system as an example, the SAVLR was able to solve the 10-day planning problem that could not be handled by most of the existing solutions. However, as the planning horizon increases, the required computer memory is significantly increased, e.g., for the 1-month planning problem, storing the transmission capacity constraints alone in the SAVLR framework would require 28.52GB memory, which is beyond the memory size of most of the personal computers. To address this issue, the SAVLR method is further improved by taking advantage of a concept called rolling horizon approach. The step-by-step implementation is given in Figure 9.

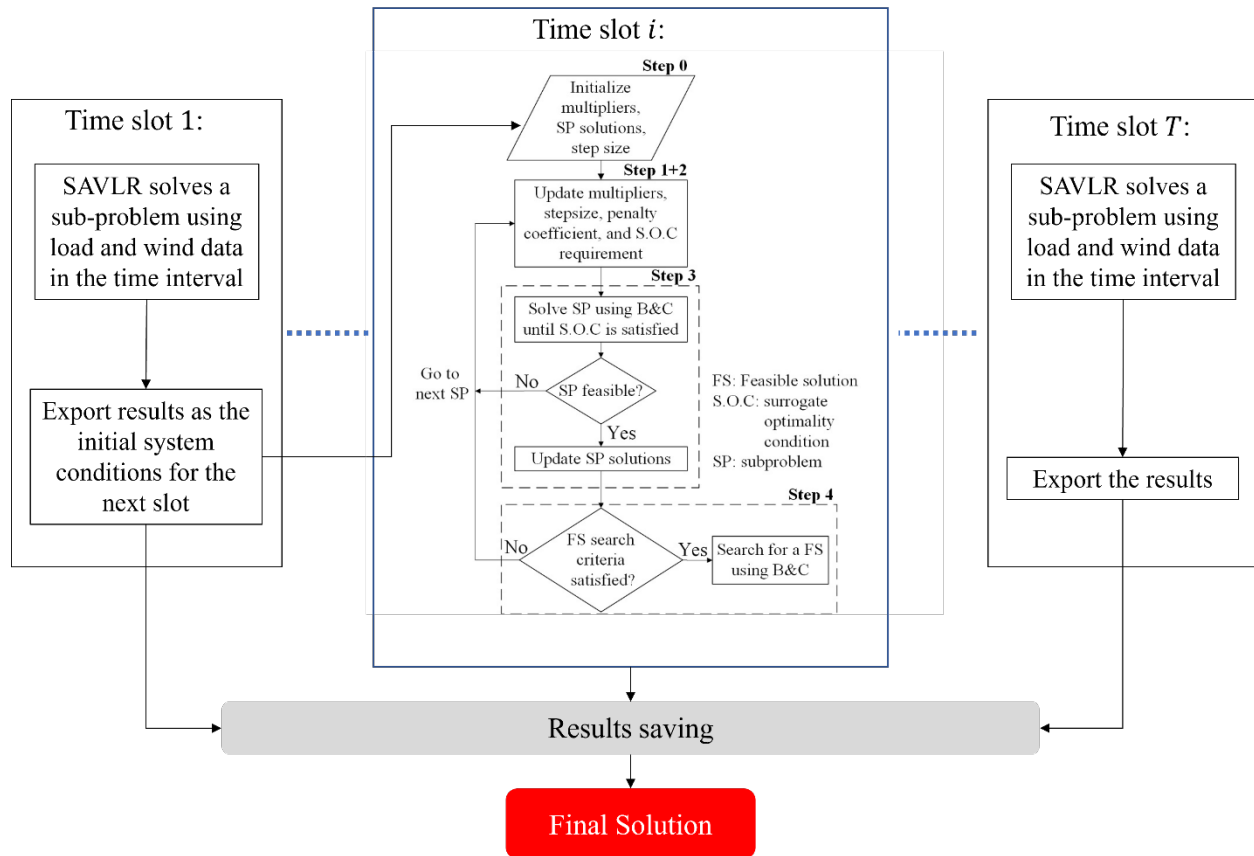


Figure 9: The flowchart of SAVLR+rolling horizon (SAVLRseq).

The rationale behind the rolling horizon approach is that, if the long-time horizon (usually more than one year) is divided into multiple shorter time slots, then it is possible that we solve the sub-problems within different time slots sequentially on a rolling basis. Instead of initializing and storing all the transmission capacity constraints and decision variables in the computer memory for the entire planning time period, the results from the previous time slot can be used as the initial conditions for the constraints and decision variables in the next time slot. In other words, the SAVLR parameters at each of the subsequent time slots

are re-initialized and the corresponding parameter values are related to the penalty multipliers of different sub-problems, resulting in a sequential version of SAVLR solution method. The problem solving for each time slot is independent of the ones in other time slots. By doing so, the implementation of the SAVLR is able to significantly save the memory requirement while maintaining a similar performance. This combination of SAVLR and the rolling horizon approach is simply named SAVLRseq (i.e., a sequential version of the SAVLR). The effectiveness of the SAVLRseq has been verified in our case studies in Section 6.

It should be noted that, in addition to these parameters in SAVLR, the SAVLRseq approach needs to carefully select the number of time slots reflecting the number of sub-problems. One could select many time slots to obtain a fast solution in each time interval. However, the large number of time slots resulting in a smaller sub-problem size may degrade the performance since the optimization solution has less future information, e.g., less forecast of load demand and wind generation to make the decisions. A tradeoff needs to be considered, as will be further discussed in Section 6.

4 ESS Operation Study

This section presents the formulation, uncertainty modeling, and the solution methodologies of the ESS operation problem developed in our ongoing papers [Raghu 2021a] and [Raghu 2021b]. More details will be presented in the papers.

The ESS operation problem can be formulated as deterministic and stochastic frequency dynamics-constrained UC problems. For the stochastic case, the uncertain wind generation is modeled as a discrete Markov process considering spatial-temporal correlation of wind speeds between multiple geographically separated windfarms. The possible wind generation states at windfarms and their probabilities of occurrence are efficiently calculated in the preprocessing stage. The formulation details are given below.

4.1 Problem Formulation

4.1.1 ESS operation with Frequency Dynamics Constraints in a Deterministic Setting

In this subsection, to examine the impacts of considering frequency dynamics on ESS operation, a deterministic wind generation scenario is considered for the frequency-dynamics constrained UC, with the RoCoF constraints (19), the linearized frequency nadir constraints (42) - (44), and QSS (33) - (34) constraints.

For this problem, a typical wind generation scenario is considered. The failure of the largest generator is considered as the contingency. The formulation details are given below.

4.1.1.1 Objective Function

The objective is to minimize unit commitment costs, i.e., on/off status and startup, as well as dispatch and penalty costs which include conventional generation, reserve, curtailment, and soft transmission capacity and reserve penalties. The objective function is formulated as:

$$\sum_{t \in \Omega_T} \left(\sum_{i \in \Omega_G} \left(c_i^{SU} SU_{it} + c_i^{NL} u_{it} + \sum_{d \in \Omega_D} c_i^{gd} P g_{it}^d + \sum_{q \in \Omega_Q} c_i^{rq} Pr_{it}^q \right) + \sum_{e \in \Omega_E} \left(c_e^{ESS, ch} B P_{et}^{ch} + c_e^{ESS, dch} B P_{et}^{dch} \right) + \sum_{w \in \Omega_W} c_w^{CUR} P_{wt}^{CUR} + \sum_{h \in \Omega_H} c_h^{P, TC} (v_{ht}^{TC+} + v_{ht}^{TC-}) + \sum_{a \in \Omega_A} \sum_{r \in \Omega_R} v_{art}^R \right). \quad (46)$$

4.1.1.2 System Constraints

In the system demand constraints, the sum of total generation, net ESS discharge power, and net wind generation must equal the total demand, and is formulated as:

$$\sum_{i \in \Omega_G} \left(\sum_{d \in \Omega_D} P g_{it}^d \right) + \sum_{e \in \Omega_E} (B P_{et}^{dch} - B P_{et}^{ch}) + \sum_{w \in \Omega_W} (Pr_{wt} - Pr_{wt}^{CUR}) = \sum_{b \in \Omega_b} P d_{bt}. \quad (47)$$

The soft transmission capacity constraints are formulated as:

$$\bar{f}_{-h} - v_{ht}^{TC-} \leq \sum_{b \in \Omega_b} \alpha_{bh} \left(\sum_{i \in \Omega_G} \sum_{d \in \Omega_D} P g_{it}^d + \sum_{e \in \Omega_E} (B P_{et}^{dch} - B P_{et}^{ch}) - P d_{bt} - \sum_{w \in \Omega_W} (Pr_{wt} - Pr_{wt}^{CUR}) \right) \leq \bar{f}_h + v_{ht}^{TC+}, \quad (48)$$

where α_{bh} are generation shift factors and $v_{ht}^{TC+/-}$ are soft constraint penalty variables to account for exceeding the constraint requirements. Other constraints not listed here for brevity include the standard unit-level, soft reserve, ESS related, and frequency dynamics, which are similar to those for the planning

problem given in subsection 3.1.2. For complete formulations of deterministic UC, see [Raghu 2021a and 2021b].

4.1.2 ESS Operation with Frequency Dynamics Constraints in a Stochastic Setting

In this subsection, the impacts of considering the Markovian wind generation model on solutions of FDUC including ESS operation are examined. For the stochastic frequency dynamics-constrained UC, the uncertain wind generation is modeled as a discrete Markov process considering spatial-temporal correlation of wind speeds between multiple geographically separated windfarms. The possible wind generation states at windfarms and their probabilities of occurrence are efficiently calculated in the preprocessing stage. The formulation details are given below.

4.1.2.1 Objective Function

The objective is to minimize one set of unit commitment costs, i.e., on/off status and startup, and a set of expected dispatch and penalty costs, i.e., conventional generation, curtailment, and soft transmission capacity penalties for each global state in the Markov model. The objective function is formulated as:

$$\sum_{t \in \Omega_T} \left(\sum_{m \in \Omega_M} p_{mt} \left[\sum_{i \in \Omega_G} \sum_{d \in \Omega_D} c_i^{gd} P g_{it}^{md} + \sum_{e \in \Omega_E} \left(c_e^{ESS, ch} B P_{et}^{ch, m} + c_e^{ESS, dch} B P_{et}^{dch, m} \right) + \sum_{w \in \Omega_W} c_w^{CUR} P_{wt}^{CUR, m} + \sum_{h \in \Omega_H} c_h^{P, TC} \left(v_{ht}^{TC+, m} + v_{ht}^{TC-, m} \right) \right] \right) + \sum_{i \in \Omega_G} \left(c_i^{SU} S U_{it} + c_i^{NL} u_{it} \right), \quad (49)$$

where m is the index for global states and p_{mt} is the probability of state m at time t .

4.1.2.2 System Constraints

Most constraints are formulated similarly to those of the deterministic problem in subsection 4.1.1. However, the constraints for the Markovian problem have increased dimensionality. To be specific, there are a set of constraints for each global state in the Markov model. For example, the system demand constraints are formulated as:

$$\sum_{i \in \Omega_G} \left(\sum_{d \in \Omega_D} P g_{it}^{md} \right) + \sum_{e \in \Omega_E} \left(B P_{et}^{dch, m} - B P_{et}^{ch, m} \right) + \sum_{w \in \Omega_W} \left(P r_{wt}^m - P r_{wt}^{CUR, m} \right) = \sum_{b \in \Omega_b} P d_{bt}. \quad (50)$$

Furthermore, ramp-rate constraints must consider all possible transitions between states at subsequent time intervals for solutions to be robust to highly varying wind speeds. For example, the Ramp-up constraints are formulated as:

$$\sum_{d \in \Omega_D} \left(P g_{it}^{md} - P g_{it-1}^{m'd} \right) \leq R U_i \cdot u_{it-1} + \left(\underline{P g}_i + \frac{R U_i}{2} \right) \left(u_{it} - u_{it-1} \right). \quad (51)$$

where the index m is for states at time t and m' is for states at time $t - 1$. The Ramp down constraints are similarly formulated. For complete formulations of the constraints, see [Raghu 2021a and Raghu 2021b].

4.2 Scenario Development: Markov Model for Wind Generation

The wind speeds at windfarms at multiple locations are modeled as a Markov chain (a discrete-state Markov process) with consideration of spatio-temporal correlations between multiple sites. The state equation for wind speeds at the different windfarms is formulated as:

$$\mathbf{w}[t + 1] = \mathbf{A} \mathbf{w}[t] + \mathbf{d}[t], \quad (52)$$

where \mathbf{w} is a truncated multivariate normally distributed random vector, \mathbf{A} is the state transition matrix where the correlation structure between windfarms is defined, and \mathbf{d} is white noise. The probabilities of

states for each time and transitions between subsequent times are calculated in MATLAB. Once wind speed states are obtained, they are mapped to wind generation states based on the non-linear wind speed to power curve of the windfarms. See Figure 10 for an example of a small Markov chain.

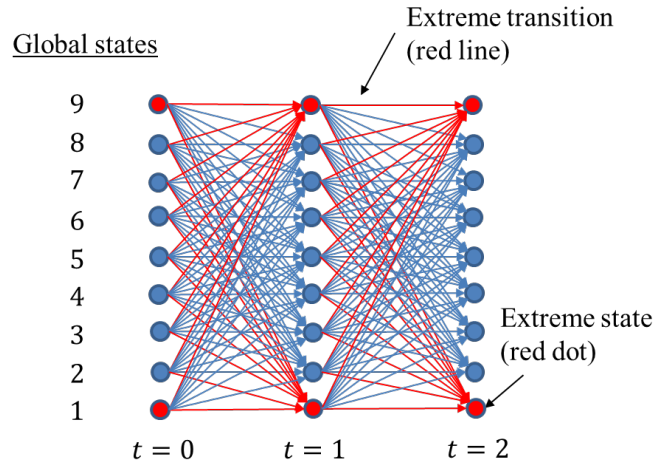


Figure 10: Example Markov chain for wind generation states for 2 hours, where $t = 0$ represents the initial distribution. This model has 9 global states (can also be considered as generation levels).

4.3 Solution

4.3.1 Solution to Deterministic ESS Operation with FDUC

To handle the high complexity due to the linearized frequency nadir constraints, SAVLR with soft constraints is used. In the subproblem formulation, only the demand and frequency nadir constraints are relaxed but not other system-wise coupling constraints to significantly reduce the number of multipliers. All other coupling constraints are converted to “soft” to facilitate coordination of subproblem solutions. For example, the RoCoF constraint is formulated as:

$$\Delta f_t^{QSS} - v_t^{QSS} \leq \Delta f_t^{QSS,max}, \quad (53)$$

where the penalty variable v_t^{QSS} accounts for violation of the constraint. The penalty variable has an associated predetermined penalty cost in the objective function. To avoid incurring excessive penalties in the solution process, the penalty coefficients are set an order of magnitude higher than the expected upper bound of multipliers. See [Raghun 2021a and Raghun 2021b] for detailed formulations.

4.3.2 Solution to Stochastic ESS operation with FDUC

To handle the high complexity of the Markovian frequency dynamics-constrained UC, a decomposition and coordination method is developed based on the SAVLR. To reduce the number of multipliers in the relaxed problem, only system demand and frequency nadir constraints are relaxed; and other coupling constraints are converted to soft constraints. To reduce computational requirements caused by the Markov process, an ordinal-optimization (OO) concept is introduced, where approximated subproblems are solved subject to the “Surrogate Optimality Condition” with much reduced complexity. Subproblems are approximated by only considering a subset of states and a subset of transitions in the original Markov model. The pseudo-code for generating states for the OO approximation is given below:

For $t = 0: T$

- Keep only up to x % (e.g., 15 %) of the upper limit of the # of global states (Keep the most likely states)
- Normalize probabilities
- For each non-zero global state:
 - If $t < T$, remove outgoing transitions from the filtered out states
 - If $t > 0$, remove transitions incoming to the filtered out states from the previous time step
 - Normalize transition probabilities for the previous time step
 - Keep y % (15 %) of most likely and extreme outgoing transitions
 - Normalize transition probabilities for the current time step
 - Based on the transition probabilities, calculate the state probabilities for the next time step

In Figures 11 and 12, the filtering method is illustrated using the example model in Figure 10.

Global states

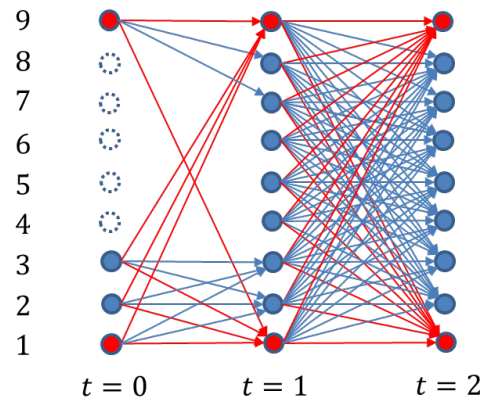


Figure 11: Active states and transitions after the first iteration of the OO filtering algorithm

Global states

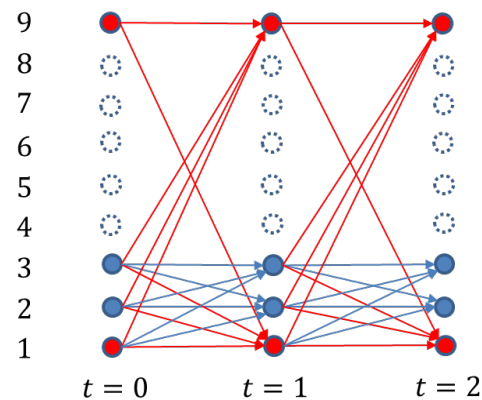


Figure 12: Active states and transitions after 3 iterations of the OO filtering algorithm

With much reduced number of states and transitions, subproblems are solved quickly until the surrogate optimality condition for the OO approximation is satisfied. At the end, feasibility is satisfied for the original

Markovian problem. To evaluate the suitability of the approximation, the surrogate optimality condition based on the original Markov model is also checked. The flow chart for the SAVLR with OO is given in Figure 13.

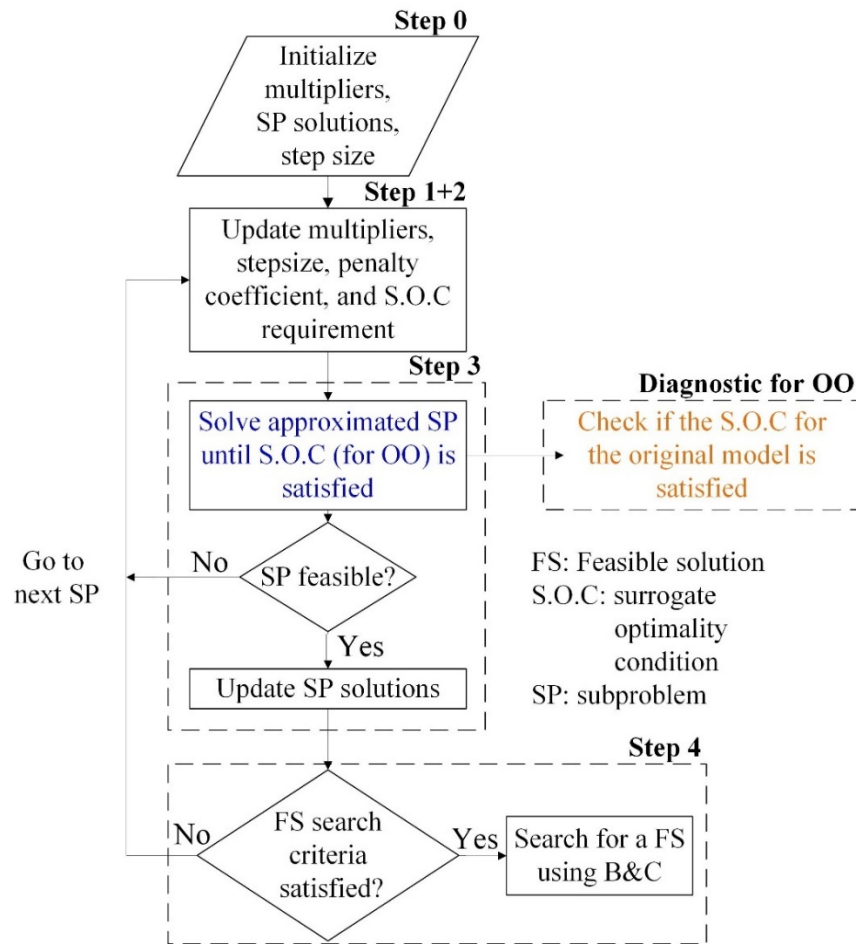


Figure 13: SAVLR flowchart with OO approximation for subproblems

5 Tool Implementation

5.1 Overall Architecture of SAVLR and SAVLRseq

The SAVLR and SAVLRseq methods developed are packaged as planning and operation tools for power systems built upon Matlab and CPLEX. The Matlab-based tools read the data files, perform the preprocessing of the data, define the optimization and constraints, implement the SAVLR via subproblem decomposition and the coordination of solving subproblems by using the state-of-practice MILP tool CPLEX. For the long-term planning problems, a so-called rolling horizon approach was developed and combined with the SAVLR to create the “SAVLRseq” tool that provides a practical solution to utility-scale long-term planning problems.

The tool implementation of SAVLR and SAVLRseq uses a fine-grained, modular, bottom-up approach to define power system models, allowing the ESS planning and operation problem to be easily formulated and customized. This architecture, as shown in Figure 14, reflects the modularity of actual power systems, where individual components operate independently but together contribute to the system’s power balance, frequency support, and total costs. In Figure 14, the MILP Modeling is the core module that defines balancing constraints for energy and reserves, frequency security, and an overall system operational cost. Other modules mainly includes *Time Scale Module* for planning and operation problems; *Component Module* for representing components such as generators, ESSs, wind farms, or transmission links; *Objectives Module* for defining the goal; *Optimization Policies Module* with different solution strategies, and the *Analysis Module*.

These modules are used together to build the overall optimization model by adding terms to the shared energy and reserve balances, frequency security, and the overall cost expression. These modules can also define additional decision variables and constraints, allowing technologies to be packaged in a plug-and-play manner that participate as fully integrated components of the overall model. Each module can be modified easily and are implemented by using user-supplied information to create a Matlab function file that is called at each stage of generating and solving a model, defining and parsing algorithm parameters, defining model components, defining costs or constraints, loading data from an input directory, and performing post-solve functions.

Following the diagram in Figure 14, users take the load and wind data as input and configure the model by a list of objective costs, constraints, and system components to be used. The tool first loads the input data (i.e., load, wind generation, and other system components); then defines the optimization model and constraints; and finally runs through compilation, solution, analysis, and export stages at runtime. This system is highly flexible, making it easy to add or subtract from the components, typically without modifying the built-in algorithm modules. By changing the choice of modules, users can also switch easily between solution functionalities, such as branch-and-cut, SAVLR, and SAVLR+rolling-horizon (i.e., SAVLRseq).

Table 5 describes the functionalities of each module. Complete mathematical formulations of the optimization model and solution algorithms can be found in the previous sections.

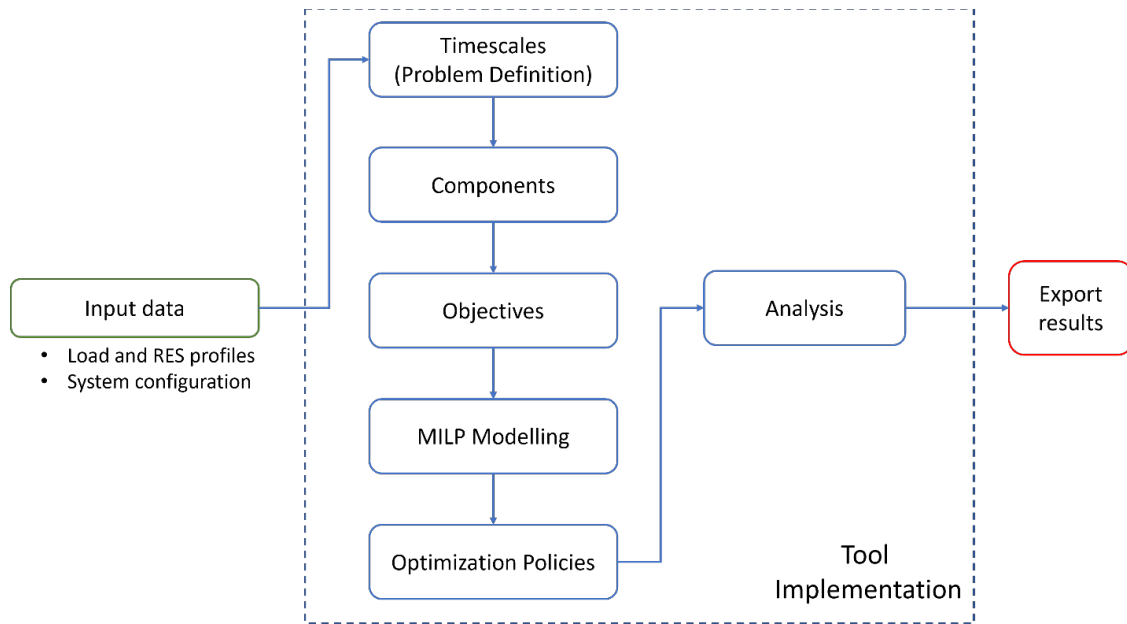


Figure 14: Structure of the open-source ESS Sizing Tool.

Table 5: The Functionality of Modules

Modules	Functionalities
Timescales	This module defines the timescales for decision making: periods of one or more years where investment decisions are made, time points within each period when operational decisions are made. Time points within each time series have a fixed duration specified in hours or minutes.
Components	This module provides the models of all possible components in a power system, including conventional generators, load demand, renewables, and ESSs. User-defined functions are allowed to specify their parameters easily.
Objectives	This module specifies the objective function and financial parameters for either the operation or planning optimization model, including investment and/or operational costs. The objective is to minimize the associated costs defined in the objective function.
MILP Modelling	This is the core module that implements the construction and operation constraints and decisions for the ESS planning and operation problems. The MILP model is developed following the convention of the unit commitment formulation. There are multiple submodules in MILP Modeling module, including power balancing, power flow, energy reserve, component capacities, demand response, and frequency security constraints. Users can flexibly decide which constraints to be included.
Optimization Policies	This module provides different solution algorithms for solving the user-specified problem. Currently, it includes branch-and-cut as the benchmark, SAVLR for operation, and SAVLR + rolling-horizon for long-time planning. The application of these solution algorithms is not limited to the mentioned examples. Users can flexibly select the solution algorithm.
Analysis	This module includes an analysis tool for evaluating the solution performance and the optimization results.

Both SAVLR and SAVLRseq are implemented in MATLAB to take advantage of vectorization and the parallel toolbox for speeding up model construction as well as implementing a parallel version of the algorithm (see [Raghun 2021a] on “Exploiting soft constraints”). CPLEX is called within MATLAB for using the B&C algorithm for solving the subproblems defined by SAVLR or SAVLRseq.

The code is lightweight and portable, and includes analytical tools for solutions. Since the code is developed in a modular style, user-defined modules can be easily added, modified, bypassed, and

debugged. Debugging features are built in to facilitate further development and customization for general MILP problems. This particular version of the code is tailored for the Markovian Frequency Dynamics- and simulated wind profile-Constrained Unit Commitment, and includes related functions.

5.2 Software Requirements

- CPLEX v12.8 or later version
- MATLAB R2018a or later version
 - CPLEX connector
 - Parallelization toolbox if parallel computation is needed

5.3 Quick Start Guide

The description of the folders and files needed for the SAVLR and SAVLRseq tools are given in Figure 15.

(Under the hood) functions:	Auxiliary functions
Original data files:	ORIGINAL DATA
Problem specific data:	Problem data
Lower bound (set manually based on B&C):	BC_LB.csv
B&C results:	BC_results.mat
Run B&C:	BC_RUN.m
Analyze B&C solution:	BC_sol_analysis.m
Define frequency and ESS parameters:	Create_FD_Data.m
Define system parameters:	Generate_instance.m
Generate Deterministic/Markovian states:	Generate_Markovian_states_transitions.m
(skip) Find unit status and generation at t(0)	get_x0_p0.m
Generate subproblems:	SAVLR_GenSPMatrix.m
SAVLR results:	SAVLR_results.mat
Run SAVLR:	SAVLR_RUN.m
Analyze SAVLR solution:	SAVLR_sol_analysis.m

Figure 15: Contents of the SAVLR code for MFDUC

```

19- load SPMatrix.mat
20
21- %% Algorithm settings
22- stepsize = 1e-2; %Initial stepsize
23- M = 10; %stepsizing parameter
24- rho_r = .1; %stepsizing parameter
25- SAVLR_c = 1; %initial savlr penalty coefficient
26- beta = 1.01; %rate of change of c
27- c_ub = 10 ; %Upper bound on c
28- run_time = 120; %Run time for algorithm
29- FS_times = [120];
30- FS_times = max(run_time,FS_times); %Times to search for feasible solution
31- nbFSsol = 3; %# of binary solutions to track
32
33- %Penalty coefficients for soft constraints
34- Pen_RoCoF = 1000;
35- Pen_QSS = 1000;
36- Pen_IRmax = 1000;
37
38- %CPLEX settings for subproblems
39- cpx_disp = 'off'; %Display engine log from subproblems
40- nbThrd = 8; % # of threads to use for subproblems
41- timelim = 10; %Time limit for SPs
42- sol_lim = 2; %# of integer solutions to find before stopping
43- MIPstart = 'on'; %Provide MIPstart for SPs (currently 100% of variables provided to MIPstart)
44

```

Figure 16: Define algorithm settings in SAVLR_RUN.m

The characteristics of the power system are stored in the “ORIGINAL DATA” folder, and problem specific modifications to the original power system data are stored in “Problem data.” Power system characteristics and load information are in “Generate_instance.m.” Frequency dynamics and ESS characteristics are defined in “Create_FD_Data.m.” Algorithm settings are defined in the run file “SAVLR_RUN.m.” Some of the parameter settings can be seen in Figure 16. Results and solution analysis tools are stored in the main folder. (In later versions of the code, they are located in a separate folder for ease of management.)

5.4 Improving Performance of MATALB Code

Parallelization and vectorization are used to speed up processing. Sparse matrices and appropriate data structures are used to minimize memory consumption. See Figure 17 for examples of parallelization and vectorization.

```

20
21 %% Algorithm settings%%...%%
49
50 %% Initialize parameters, vectors, and indices%%...%%
86
87 %% Construct SP constraint matrices in parallel
88
89 fprintf('Constructing subproblem constraint matrices...\n\n')
90 tic
91 parfor i = 1:nbSP
92     [sp_data] = ParInitSPinfo(Constant_Data, i, log_idx);
93     SP_Data{i} = sp_data;
94 end
95 oh_init = toc; %overhead
96 [hours, mins, secs] = sec2hms(oh_init);
97
98 fprintf('Overhead: %.2g s\n\n', secs)
99
100 %% SAVLR iterations (Solve SP, extract SP solutions, update
1088 %RoCoF constraint
1089 if LG_SP == 1
1090     S_i = [];
1091     S_j = [];
1092     v = [];
1093     cnt = 0;
1094     for t = 1:T
1095         num_t_states = length(state_filt{t+1});
1096         for n = 1:num_t_states
1097             cnt = cnt+1;
1098             S_i(end+1:end+SP_nbUnits+1) = cnt*ones(1,SP_nbUnits+1);
1099             S_j(end+1:end+SP_nbUnits+1) = [p_ess_IR_idx{t}(n), x_idx{1:LG_idx
1100             v(end+1:end+SP_nbUnits+1) = [-1, (-2*RoCoF_max+H/f0)*Pmax(SP_unit
1101
1102         end
1103     Aineq17 = sparse(S_i, S_j, v, max(S_i), nbVars);
1104     INEQ_cnst_idx{17} = INEQ_cnst_idx{16}(end)+1:INEQ_cnst_idx{16}(end) + max
1105     % INEQ_cnst_idx{17} = INEQ_cnst_idx{16}(end);
1106
1107 else
1108     S_i = [];

```

Figure 17: a) parallel for loop is used for constructing subproblem models in the preprocessing stage. b) The RoCoF constraints are built using vectorization and stored in a sparse matrix.

6. Case Study

6.1 Example Systems

Two example systems were used in the case study, i.e., the IEEE 118-bus system¹ and the 2,383-bus Polish system [MATPOWER]. The two systems were modified and used to illustrate the effectiveness of the ESS planning and operation models and the SAVLR-based solution methodology.

The IEEE 118-bus system, as shown in Figure 18, represents a simple approximation of the system of the American Electric Power system and has often been used in various studies. The system contains 19 generators, 35 synchronous condensers, 177 lines, 9 transformers, and 91 loads.

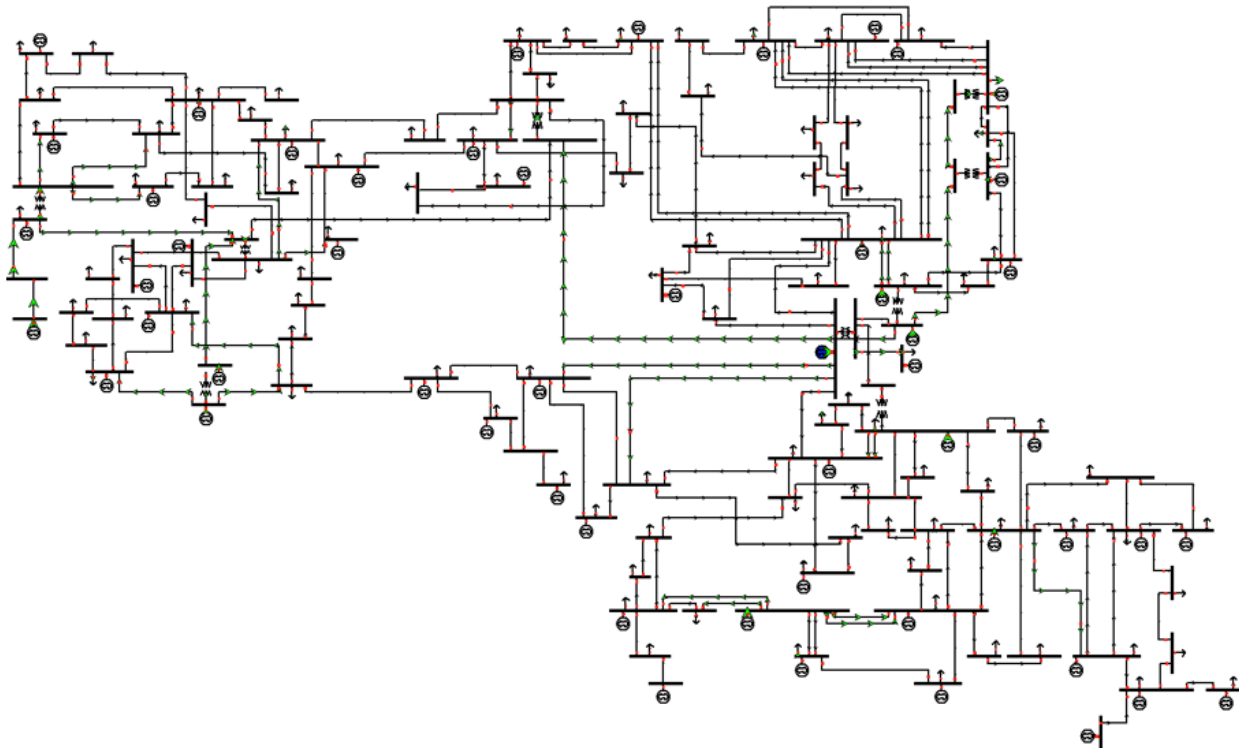


Figure 18: Diagram for the 118-bus system.

The Polish system [MATPOWER] represents the Polish 400, 220 and 110 kV networks during winter 1999-2000 peak conditions. It is part of the 7,500+ bus European UCTE system. The system contains 327 generators and 2896 transmission lines.

6.2 ESS Operation Case Study

6.2.1. ESS Operation in a Deterministic Wind Generation Setting

In this case study of the deterministic ESS operation problem of the 2,383-bus Polish system, it is assumed that three wind farms are connected to buses 9, 21, and 62 and the ESSs are installed at buses 180, 1016, and 681.

A 24-hour frequency dynamics-constrained UC with ESSs is solved to demonstrate the role of ESSs in providing grid inertia support as well as peak shaving and reserve services. The details of this study is being

¹ Details of the system and data are available at http://labs.ece.uw.edu/pstca/pf118/pg_tca118bus.htm.

documented in a journal paper [Raghu 2021a]. The SAVLR obtains a solution with cost \$31,340,000 with a gap of 2.67%. By considering frequency dynamics in UC, more conventional units are online at an additional cost of \$840,000 to help provide grid inertia and maintain the system frequency at safe levels during contingencies. Figure 19 compares the behavior of ESSs with and without frequency constraints.

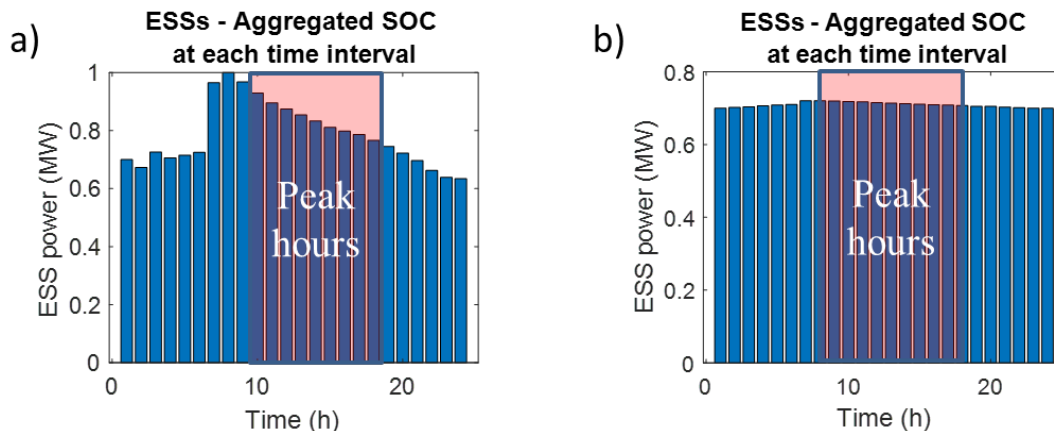


Figure 19: Aggregated state-of-charge of ESSs for the deterministic FDUC

In Figure 19 a), without frequency dynamics constraints, the ESSs charge during the early morning hours, and then discharges during peak hours to reduce the load for conventional generators, i.e., the major role of the ESSs is peak-shaving. In Figure 19 b), with frequency dynamics considered, much of the ESS power is conserved to provide inertia support for contingencies while the system demand is mainly supplied by conventional generators and wind farms.

6.2.2. ESS Operation for the Markovian wind generation model

The IEEE 118-bus system is used in this study. The wind farms are assumed to be connected to buses 9, 21, 62, and the ESSs are installed at buses 117, 21, 82.

A 24-hour Markovian frequency dynamics-constrained UC with ESSs is solved to demonstrate the role of ESSs in providing grid inertia support. SAVLR with the ordinal optimization concept embedded subproblem solving is used, where 10% of the number of possible states and 10% of the number of possible transitions are kept (referred to as SAVLR+OO-10/10).

Two cases are examined: a low wind case with the initial wind speed distributed around 2m/s at all windfarms, and a high wind case with the initial wind speed distributed around 10 m/s at all windfarms. These cases are compared with the two extreme deterministic cases with no wind and maximum wind generation. The feasible costs and algorithm performance metrics are given in Table 6.

Table 6: Results from SAVLR+OO for the Markovian FDUC

Method	Feasible cost (\$)	Solution time	~ SP solve time	# maj. iter.
Deterministic extreme cases (Solved by B&C)				
BC – det., no wind	985,315	22 s	-	-
BC – det., max wind	906,911	40 s	-	-

Markovian - Case 1 (Low wind)				
SAVLR+OO-10/10	981,780	~12 m	8.5 s	5
Markovian - Case 2 (High wind)				
SAVLR+OO-10/10	937,033	~16 m	29 s	3

For the Markovian cases, SAVLR+OO-10/10 finds solutions within 20 minutes. For the Markovian low wind case, SAVLR+OO finds a solution that is only \$3,535 cheaper than the deterministic case with no wind. This is because when low wind speed is expected, conventional generation still provides the majority of power, thus savings are small. With higher expected wind speed, the load on conventional generators decreases and leads to savings of \$48,282. Unlike solutions for deterministic cases, the solutions for Markovian cases are guaranteed to be feasible even when there are extreme transitions between global states. In-depth analysis of the results is being performed to analyze the impacts Markovian wind generation on the behavior of ESSs and will be documented in [Raghu 2021b]. Further applications of the ordinal optimization concept by separating uncertainties within a particular windfarm from uncertainties from all other windfarms is being considered to push for additional scalability.

6.3 ESS Planning Case Study

6.3.1. Test Systems and Data

It is assumed that there are three wind farms as well as three ESSs installed in each of the example systems. For case studies, it is assumed that three wind farms are installed at buses 4, 5 and 6 in the 118-bus system and at buses 9, 21 and 62 in the Polish system, respectively.

The uncertainties of load and wind power profiles were developed to represent different scenarios over one year horizon. The load data adapted from [ERCOT, 2020] are appropriately scaled. The wind speed data is generated by the Random Field method described in Section 3.2 and converted to wind generation, as shown in Figure 20, by using Eq. (54).

$$Pr = \frac{1}{2} \rho A_w v^3 C_p \quad (54)$$

where ρ , the density (kg/m^3) is 1.23; A_w , the swept area (m^2) is 8,495; C_p , the power coefficient is 0.59 by assuming wind turbines operate at maximum power point tracking (MPPT). In the case studies, we used these wind generation profiles as the scenarios.

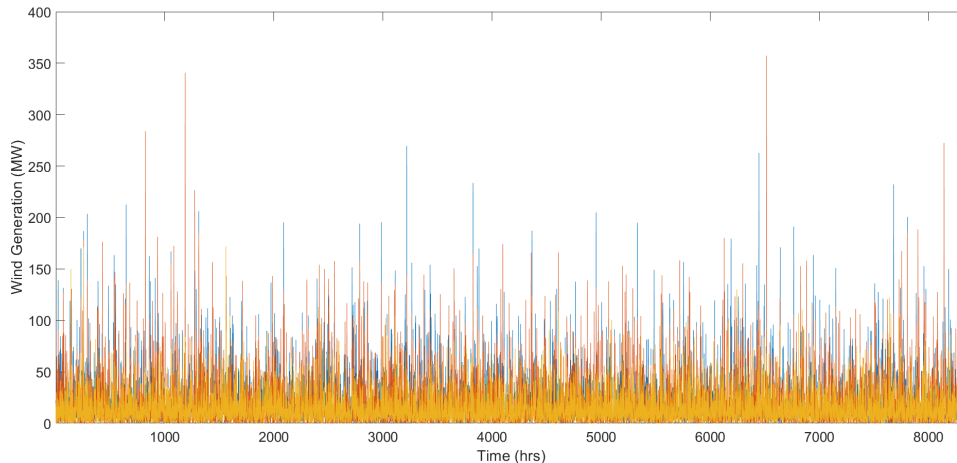


Figure 20: Wind generation obtained by Random Filed.

The rolling horizon approach provides an effective means to avoid the memory issue. However, its time interval affects the performance and needs to be carefully selected. To avoid the complication of solving the UC problem, the rolling horizon approach is only adopted for long-time planning (e.g., one year), where we expect the issue of insufficient the PC memory.

6.3.2. Tuning Parameters

There are parameters (i.e., M , γ , and step size) that need to be tuned in the SAVLR solution method to achieve the best performance before implementing the solution. Specifically, we first fix γ at a value based on our experience, and we tune the M and step size each in a given range. The parameters with the best performance were used for all the test cases. The results given in Table 7 were obtained by applying the SAVLR to a short-time planning problem (e.g., 3 hours) for the IEEE 118-bus system.

Table 7: Comparison of different parameters for the 3-hrs planning problem ($\gamma = 0.1$).

	Step size = 1×10^{-3}	Step size = 5×10^{-3}	Step size = 1×10^{-2}
$M = 1.0$	57874 (19s)	57874 (29s)	59096.9 (5.4s)
$M = 10$	57874 (17s)	56481 (20s)	59235.4 (3.7s)
$M = 20$	57874 (17s)	58739.9 (12s)	59235.4 (2.1s)

The SAVLR performance is measured by using the feasible cost solved within a specified time limit (e.g., 30s). If it cannot return a feasible cost within this time limit, we consider it as NaN. The best parameters for each system are highlighted, i.e., $M = 10$, $\gamma = 0.1$, and stepsize = 5×10^{-3} .

6.3.3. Results

All the planning problems were solved using a Dell laptop computer with an 8-core intel i9 CPU and 32GM RAM memory.

6.3.3.1. IEEE 118-bus System: 24-hour Planning Problem

We first applied the original SAVLR to solve a 24-hour planning problem. The optimization result for the IEEE 118-bus system is described below. The total costs are $\$5.6301 \times 10^5$. The upper bound of the BESS maximum charging/discharging power is set to be 170 MW at each bus. The result is that we should invest to build ESSs of capacity 166.66 MW at bus 4, 168.63 MW at bus 2, and 170 MW at bus 3, respectively. The 24-hour profile of generation output from conventional generators, wind power, BESS discharging, and load shedding is shown in Figure 21. Figure 21 indicates that the power generation is mainly from the conventional generators and wind power. The power generation from BESS discharging is insignificant, and there is no need for load shedding in this situation.

It is interesting that the total BESS installation capacity is 505.29 MW while the total discharging power in each hour is very small. The reason is as follows. Since the BESSs are responsive, they are scheduled to decrease the charging power and/or increase the discharging power, and this can avoid the frequent charging and discharging and increase the lifespan of the BESSs. Therefore, the BESSs are scheduled to operate in a standby mode to be ready for providing frequency support in case a contingency occurs.

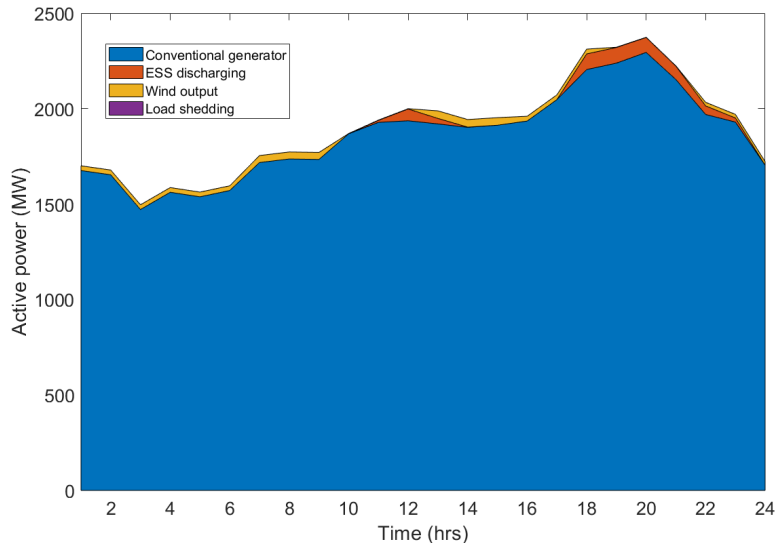


Figure 21: Results for 24hrs planning with ESS support.

We also tested the impacts of removing the BESSs from the system. As in Figure 22, more load has to shed when the BESSs are removed from the system. Without deployment of ESSs, there is insufficient fast generation for provisioning frequency support, and the system would have to shed additional loads to satisfy the frequency constraints.

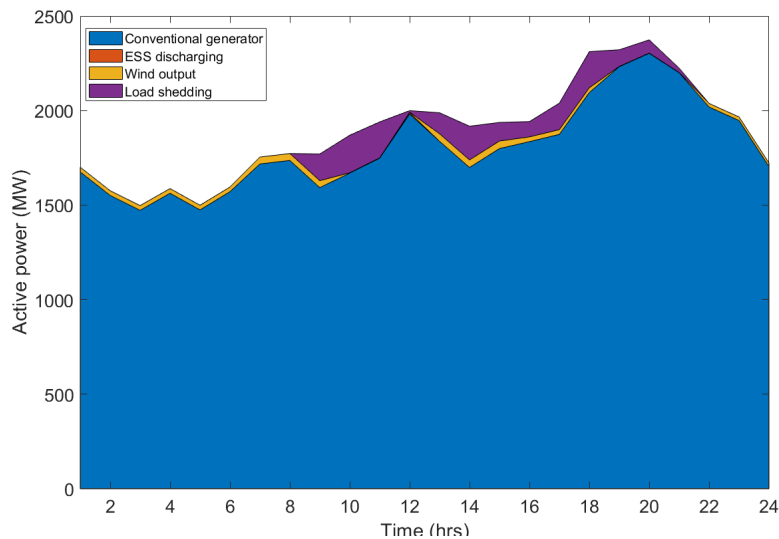


Figure 22: Results for 24hrs planning without ESS for frequency support.

6.3.3.2. IEEE 118-bus System: One-year Planning Problem

Before solving the one-year planning problem, we first tested the performance of the rolling-horizon approach by comparing the results of the combination of the SAVLR and rolling horizon, i.e., SAVLRseq method, to the SAVLR alone and branch-and-cut (B&C) methods for solving the one-month (i.e., 720hrs) planning problem. In Table 8, all the algorithms can find feasible solutions. Compared to the SAVLR and B&C methods, a combination of the SAVLR and rolling-horizon can have a similar performance while significantly reducing the solution time as well as the memory (not shown in Table 8). This feature provides

us with a practical alternative to address the memory issue that is unavoidable when solving the long-term UC based planning problems.

Table 8: Comparison of different solutions for the one-month planning problem.

Method	Feasible cost	Solution time
Branch-and-cut	1.9655×10^7	1h30m
SAVLR	1.9749×10^7	13m50s
SAVLR + Rolling-horizon	1.9787×10^7	6m30s

When applying the SAVLRseq, an additional parameter, the number of time slots across the entire planning horizon, needs to be selected, as indicated in Section 3. This is illustrated by one case study using the IEEE 118-bus system for a 240-hour planning as an example, and the results are shown in Table 9, where the gaps are calculated based on the lower bound obtained by branch-and-cut. It is shown that although increasing the number of time slots decreases the solution time, the quality of the results would be affected. Therefore, there is a trade-off between the quality and computational time when applying SAVLRseq, and we only apply it to the problem when both branch-and-cut and original SAVLR cannot find feasible results, e.g., the long-time planning problem of a large-scale system. The recommendation is that the number of time slots can be chosen such that the available memory is fully employed.

Table 9: Comparative results of SAVLRseq with different time slots.

Method	Lower bound	Feasible cost	Gap	Solution time
Branch-and-cut	5.8453×10^6	5.8954×10^6	0.85%	8m30s
SAVLRseq (10 time slots)	\	6.0437×10^6	3.28%	2m20s
SAVLRseq (4 time slots)	\	6.0194×10^6	2.89%	4m08s

We then applied the SAVLRseq to solving the one-year planning problem for sizing the ESSs. The B&C method cannot find any lower bound and feasible solution in this case for the original problem. To obtain a lower bound, we have to simplify the problem by removing transmission capacity constraints. The comparative results are summarized in Table 10, where the lower bound is obtained by solving the simplified problem via the branch-and-cut method. Note that the results for both SAVLR and SAVLRseq are obtained by solving the original problem.

Table 10: Comparison of different solutions for the one-year planning problem in 118-bus system.

Method	Lower bound	Feasible cost	Lower bound finding time	Solution time
Branch-and-cut	2.286×10^8	\	15m40s	\
SAVLR	\	2.3579×10^8	\	50m30s
SAVLR + Rolling-horizon	\	2.3617×10^8	\	37m28s

Table 10 shows that the SAVLRseq is able to find the solution much faster than using SAVLR alone with comparable quality. The profile of generation output from conventional generators, wind power, BESS discharging, and load shedding are shown in Figure 23. Figure 23 shows that the power generation is again mainly from conventional generators and wind power, and contribution to the total generation from the BESSs is very small and, therefore, can hardly be seen in the figure. There is no load shedding needed in this situation. The results also indicate that the combined SAVLR and rolling horizon approach has a great potential to be applied to large-scale systems.

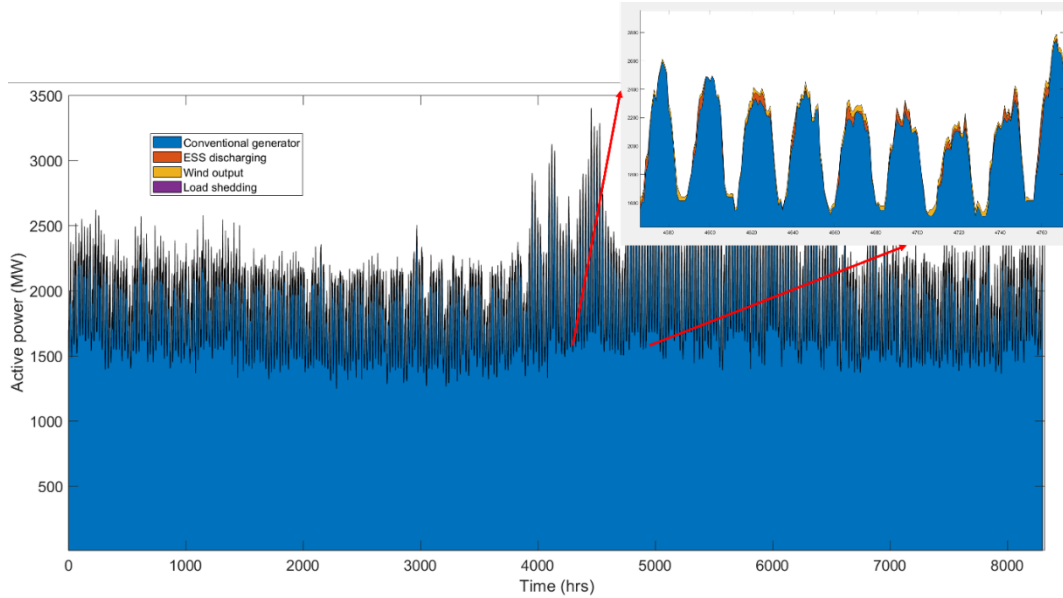


Figure 23: Figure 4. Results for one-year planning with ESS for frequency support

6.3.3.3. Scalability Study in the 2,383-bus Polish System: 24-hrs Planning Problem

Similar to the study using the IEEE 118-bus system, we first applied the original SAVLR to solve a 24-hrs planning problem for the Polish system. The optimization result for the Polish system was successfully obtained by using the SAVLR and is described below.

The total costs are $\$5.1747 \times 10^7$. The upper bound of each BESS' maximum charging/discharging power is set to 1,050 MW. The investment results are the deployment of 1,000.50 MW at bus 180, 960.70 MW at bus 1016, and 1,050 MW at bus 681, respectively. The 24-hour profile of generation output from the conventional generators, wind power, BESS discharging, and load shedding is shown in Figure 24. Figure 24 again shows that the power generation is mainly from conventional generators and wind power, the contribution of BESSs is insignificant, and load shedding is zero. The results are consistent with the findings in the case study of the IEEE 118-bus system. The discharging power from the BESSs is not much due to need to be ready for providing the frequency support.

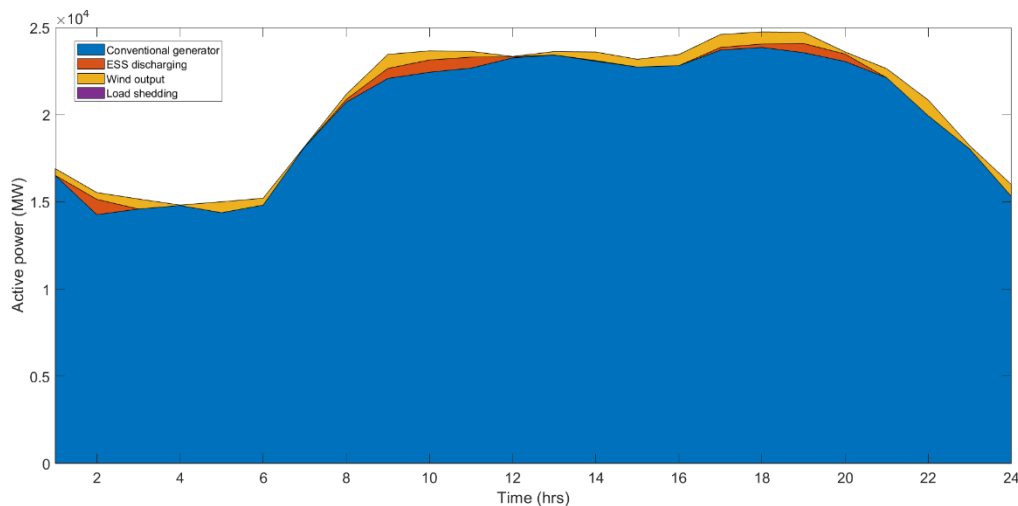


Figure 24: Results for 24-hrs planning with ESS for frequency support.

6.3.3.4. Scalability study in the 2,383-bus Polish system: One-year planning problem

As proved by the test in the IEEE 118-bus system, directly solving the long-term planning problem for a large-scale system would be time-consuming and often impossible. For example, for the one-month planning problem, it needs 28.52GB of memory to store the transmission capacity constraints only. Therefore, it is impossible to solve the one-year planning problem on a PC. Even the original SAVLR cannot find the solution given a long-term planning problem of a relatively large system due to the limited memory. By combining the SAVLR and the rolling-horizon approach, the solution can be obtained within 51 hours using a 48-hour interval, as summarized in Table 11.

Table 11: Comparison of different solutions for the one-year planning problem in Polish system.

Method	Lower bound	Feasible cost	Lower bound finding time	Solution time
Branch-and-cut	\	\	\	\
SAVLR	\	\	\	\
SAVLR + Rolling-horizon	\	1.7896×10^{10}	\	50h43m02s

The results in Table 11 verify that only the SAVLRseq approach can solve this one-year planning problem for the Polish system.

Due to the unavailability of utility system planning model, the combined SAVLR and rolling horizon approach has not been tested to large systems. However, based on the studies we performed so far, we are confident that the model and the solution developed in this project can be applied to long-term planning for utility-scale systems.

7. Conclusions and Future Work

In this project, we developed a scalable methodology and a practical tool that can be used by utilities to perform UC-based ESS planning and operation to guarantee a reliable and secure operation of large-scale power systems by satisfying various constraints, including those related to frequency dynamics, under high uncertainties associated with the continually increasing renewables.

Two closely connected topics were studied in this project, i.e., sizing of ESSs considering constraints such as frequency responses under high penetration of renewables and stochastic operation optimization of ESSs accounting for SOC and intermittence of renewable generation and the increasing load uncertainties due to, e.g., behind-the-meter renewables (e.g., rooftop PVs). The frequency response-based ESS sizing and stochastic optimization-based operation ensure the frequency stability and reliability of the system via the efficient operation of ESSs together with other units in the grid. The study was enabled by the development and implementation of an innovative scalable stochastic optimization method, which consists of more realistic uncertainty modeling, constraint tightening, a decomposition and coordination based SAVLR that can be combined with an ordinal optimization and a rolling horizon approach, to solve MILP problems including utility-scale UC problems.

The study shows the critical role that ESSs play in improving system reliability and stability by providing inertia support in low inertia conditions, especially under intermittent wind generation. ESSs also provide, to a lesser extent, peak shaving and reserve services to improve the economic efficiency of grid operation. This study is an important step to economic accommodation of more renewable generation via the assistance of ESSs while maintaining stability of the grid dynamics under various disturbances and uncertainties.

The major contributions of this study include:

- i. Development of the Markovian approach-based model and RFT-based approach for a more realistic representation of wind generation related uncertainties that are suitable for ESS operation and planning studies by considering both spatial and temporal evolutions of wind speed information
- ii. Performance of a systematic constraint tightening approach that may significantly simplify the computational requirements to solve MILP problems
- iii. Refinement of a scalable Surrogate Absolute-Value Lagrangian Relaxation method that can be easily scaled up for large systems via a decomposition and coordination approach
- iv. Development of rolling horizon-based concept that can be used together with the SAVLR to create the SAVLRseq approach that enables practical solutions to long-term planning problems without requiring high performance computing (HPC) facilities
- v. Introduction of an ordinal-optimization (OO) concept to approximately solve a Markovian subproblem in ESS operation via simplified models with much reduced complexity while maintaining the quality of the overall solution
- vi. Implementation of the SAVLR and SAVLRseq in an open-source, modular, and flexible tool that is readily used for solving utility-scale UC problems.
- vii. An initiation of the development of an innovative integrated mathematical optimization and machine learning (ML) method, i.e., a ML-assisted SAVLR or ML-SAVLR, to address the complexity of the optimal planning and operation.

The methodology and the tools developed have been successfully applied in this study to perform frequency dynamics constrained ESS sizing and operation using two example systems, i.e., the IEEE 118-bus system and the 2,283-bus Polish system. ESSs are demonstrated to provide valuable grid inertia support, and, to a lesser extent, peak shaving and reserve services to improve the economic efficiency of grid operation.

A number of conclusions and insights has been achieved in the study:

- i. Responsive ESSs play a critical role in improving the stability and reliability by providing frequency support in low inertia conditions, especially under intermittent wind generation.
- ii. Without deployment of ESSs, load shedding may be unavoidable due to intermittency when the penetration level of the wind generation is high, even without generator outages. This is mainly because of the insufficient fast generation for provisioning the frequency support.
- iii. Realistic uncertainty modeling must be performed by not only considering the spatial and temporal correlations of environmental conditions such as wind speed, precipitation, solar irradiance, temperature, but also the trend of the variations in these conditions. The RFT-based and the Markovian approaches are capable of capturing the correlations and trend of the weather conditions and the renewable generation profiles.
- iv. When considering the frequency constraints including frequency nadir, rate of change of frequency, and quasi-steady-state frequency responses, the complexity of the UC based ESS planning and operation problems increases tremendously.
- v. Solving the frequency dynamics constrained UC problems for ESS planning and operation is beyond the capability of the existing stochastic optimization methods except the SAVLR and SAVLRseq developed in this study.

Additional studies are identified and presented here.

- i. Popular battery technology-based energy storage systems are considered in this study. The methodology and the tools developed can be further extended to evaluate ESSs of different technologies such as flywheel, pump hydro, supercapacitor.
- ii. The frequency constraints related to frequency nadir, RoCoF, and QSS were derived based aggregated system wind equations and are actually conservative, which will lead to conservativeness in the investment and installation of ESS capacities. This can be further investigated and improved in the future studies.
- iii. The ESS planning and operation studies can be investigated by further considering the solar generation as well as the possible correlation between wind and solar resources.
- iv. The SAVLR and SAVLRseq tools can be further tested by applying to the planning and operation of ISO-scale systems.
- v. The ML-assisted SAVLR method will be continually developed and further enhanced by developing a distributed and asynchronous version and extending the theoretical results from centralized coordination to distributed coordination while aiming at large-scale implementation.

It should also be noted that the methodology and tool developed are not limited to ESS planning and operation problems. They can also be tailored and used for solving generic stochastic optimization problems. The study in this project is an important step for economically and reliably accommodating more renewable generation via the assistance of ESSs while maintaining stability of the grid dynamics under various disturbances and uncertainties.

References:

- [Bragin 2019] M. A. Bragin, P. B. Luh, B. Yan, and X. Sun, "A Scalable Solution Methodology for Mixed-Integer Linear Programming Problems Arising in Automation," IEEE Transactions on Automation Science and Engineering, Vol. 16, No. 2, April 2019, pp. 531-541, DOI: 10.1109/TASE.2018.2835298. 2020 Best Transactions Paper Honorable Mention.
- [CAISO] "What the duck curve tells us about managing a green grid," available at https://www.caiso.com/Documents/FlexibleResourcesHelpRenewables_FastFacts.pdf.
- [Chavez 2014] H. Chavez, R. Baldick, and S. Sharma, "Governor rate-constrained OPF for primary frequency control adequacy," IEEE Trans. Power Syst., vol. 29, no. 3, pp. 1473-1480, 2014.
- [ERCOT 2020] "ERCOT Hourly Load Data Archives," available online at http://www.ercot.com/gridinfo/load/load_hist/ [Vanmar 2010] E. Vanmarcke (2010). *Random Fields: Analysis and Synthesis*. World Scientific Publishing Company.
- [Luh 2020] P. Luh et al, "Frequency Dynamics Constrained Unit Commitment for Reliable Power System Operation," Presentation in Panel Session of Improving the efficiency of large-scale Unit Commitment towards future resource Integration, IEEE PES GM, August 2020.
- [MATPOWER] <https://matpower.org/docs/ref/matpower5.0/case2383wp.html>.
- [Papale 2019] S. M. Papalexiou and F. Serinaldi, "Random Fields Simplified: Preserving Marginal Distributions, Correlations, and Intermittency, With Applications from Rainfall to Humidity," Water Resources Research, 2019.
- [Raghun 2021a] N. Raghunathan et al, "Frequency Dynamics Constrained Unit Commitment with Energy Storage Systems," manuscript completed and to be submitted.
- [Raghun 2021b] N. Raghunathan et al, "Markovian Frequency Dynamics Constrained Unit Commitment with Energy Storage Systems," manuscript completed and to be submitted.
- [RF] "Random Fields," available online at https://statweb.stanford.edu/~jtaylo/courses/stats352/notes/random_fields.pdf
- [Tsouka 2020] I. Tsoukalas, P. Kossieris, and C. Makropoulos, "Simulation of Non-Gaussian Correlated Random Variables, Stochastic Processes and Random Fields: Introducing the anySim R-Package for Environmental Applications and Beyond," Water 2020, 12, 1645; doi:10.3390/w12061645.
- [Wan 2011] Y.-H. Wan, "Analysis of Wind Power Ramping Behavior in ERCOT," Technical Report, NREL/TP-5500-49218, March 2011.
- [Yan 2020] B. Yan, P. B. Luh, T. Zheng, D. Schiro, M. A. Bragin, F. Zhao, J. Zhao and I. Lelic, "A Systematical Formulation Tightening Approach for Unit Commitment Problems," IEEE Transactions on Power Systems, Vol. 35, No. 1, January 2020, pp. 782-794, DOI: 10.1109/TPWRS.2019.2935003.
- [Yue 2015] M. Yue and X. Wang, "Grid Inertial Response-Based Probabilistic Determination of Energy Storage System Capacity under High Solar Penetration," IEEE TRANSACTIONS ON SUSTAINABLE ENERGY, VOL. 6, NO. 3, JULY 2015.
- [Yue 2018] M. Yue, S. W. Kang, J. Jin, and J. Matevosjana, "An Investigation of Potential Intermittency Induced Outage Modes for Wind Generation," PMAPS 2018.

[Zhan 2019] J. Zhan, M. Yue, and L. Fan, "Reliability-Based Stochastic Transmission Expansion Planning Considering Uncertainties of Dynamic Thermal Rating and Wind Power," IEEE PES GM 2019.

[Zhao 2021] T. Zhao, M. Yue, and P. B. Luh. "A scalable stochastic optimal planning of Energy Storage Systems Considering Frequency Dynamics." Paper completed (2021)